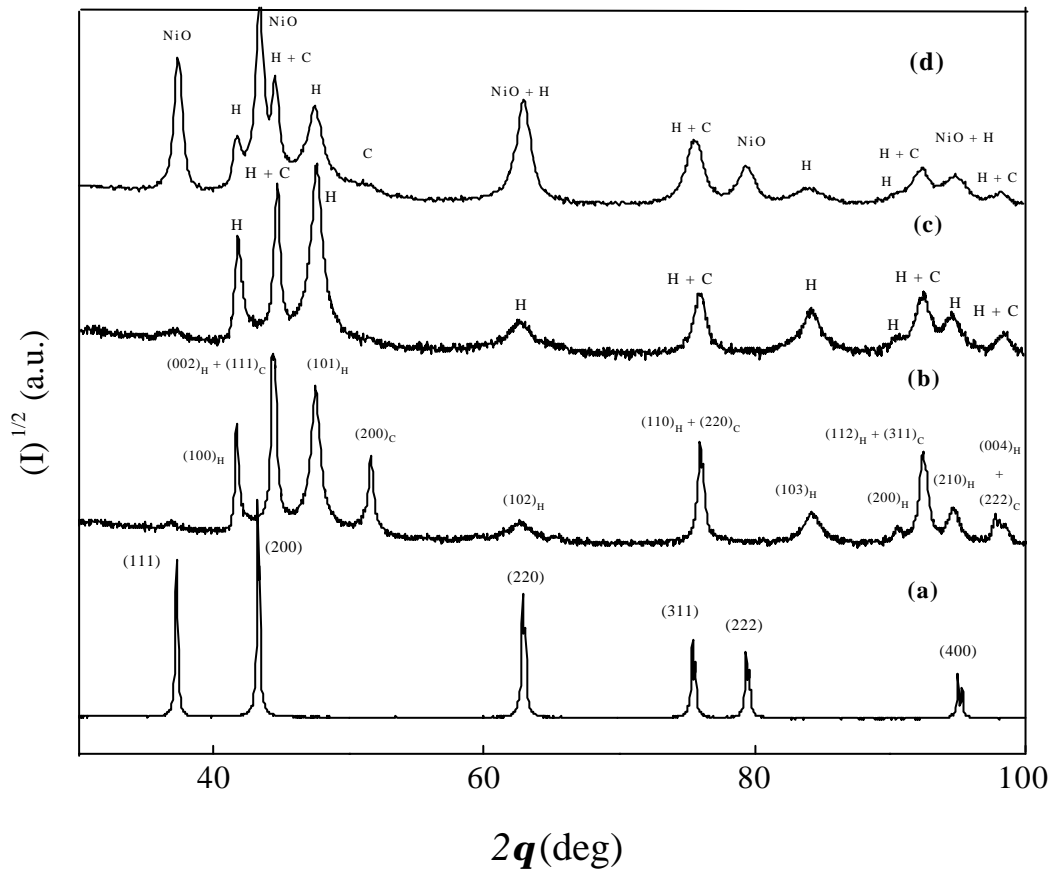


### 3.2.2.- The structure evolution of Co ball milled with NiO

Shown in figure 3.11 are the XRD patterns of unmilled NiO (a), unmilled Co (b), 1 h ball milled Co (c) and 20 h ball milled Co + NiO (d). The XRD pattern of Co ball milled with NiO for 20 h, together with the curve generated from the full pattern fitting procedure and the corresponding difference between the calculated and the experimental profiles can be seen in figure 3.12, which reveals that the quality of the fit is rather good. The XRD pattern of NiO is the typical of a fcc structure. However for Co, as in ball milled Co alone, a mixture of two phases, hcp + fcc, is observed. The subindexes H and C in figure 3.11 denote hcp and fcc Co, respectively. The Miller indexes ( $h,k,l$ ), for both Co and NiO, are also indicated in the figure.



**Figure 3.11:** XRD patterns of (a) unmilled NiO, (b) unmilled Co, (c) 1 h ball milled Co and (d) 20 h ball milled Co + NiO in the weight ratio 1:1.

When Co is milled together with NiO the intensity of fcc-Co diffraction peaks also decreases with milling time, indicating that the transformation from fcc to hcp-Co also takes place. Moreover, XRD peaks are found to broaden progressively as the milling time increases. This is due, like for Co milled alone, to the decrease of crystallite size and the increase of microstrains. Some representative structural parameters, obtained from the full-pattern fitting procedure (Rietveld method) of Co ball milled with NiO in the weight ratio of 1:1 are shown in Table 3.2. Note that since the fcc content is very small it is impossible to determine the milling time evolutions of the crystallite size and microstrains of the fcc phase.

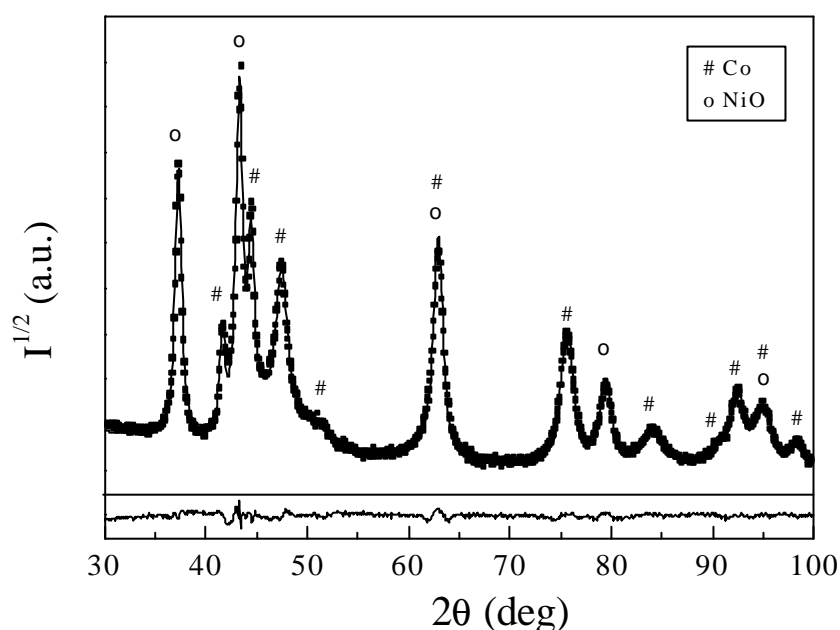


**Figure 3.12:** X-ray diffraction pattern of Co ball milled with NiO for 20 h in a weight ratio of 1:1, together with the curve generated from the full pattern fitting procedure and the corresponding difference between the calculated and the experimental profiles. The symbols # and o denote Co and NiO peaks, respectively.

It is important to point out that in Co ball milled with NiO (in the ratio 1:1), some of the structural changes occurring in Co during the milling slow down compared to Co milled alone [1,2]. For example, the minimum fcc content in ball milled Co + NiO is observed after milling for 20 h, instead of 1 h as for Co milled alone (compare table 3.2 with figure 3.8). Also the stacking fault probabilities in the 20 h ball milled Co + NiO resemble those of 1 h ball milled Co (compare table 3.2 with figure 3.10). It is noteworthy that the overall stacking fault probability in Co ball milled with NiO, i.e.  $a_H + b_H$ , increases with milling time more

slowly than in ball milled Co alone. However, as in the case of ball milled Co, the major changes in the hcp-Co crystallite size,  $\langle D \rangle_H$  and microstrains,  $\langle e^2 \rangle_H^{1/2}$ , occur during the first stages of milling (note from Table 3.2 that the values of  $\langle D \rangle_H$  and  $\langle e^2 \rangle_H^{1/2}$  in the 20 h and 30 h ball milled Co + NiO are relatively similar, compared to the changes occurring for shorter milling times). However, it should be noted that the values of  $\langle D \rangle_H$  in Co + NiO milled for several hours become somewhat smaller than in Co milled alone.

It is also remarkable that during ball milling the positions of the XRD peaks, for both Co and NiO remain essentially unchanged, indicating that the cell parameters do not change substantially. Therefore, the amount of atomic interdiffusion between both components is small, as has been also deduced from EDX analyses of Co-NiO composites.

Milling Time	$\langle D \rangle_H$ (nm) ( $\pm 0.3$ )	$\langle e^2 \rangle_H^{1/2}$ ( $\pm 0.1 \times 10^{-3}$ )	$a_H$ ( $\pm 0.002$ )	$b_H$ ( $\pm 0.003$ )	% fcc (weight) ( $\pm 1$ )	$\langle D \rangle_{NiO}$ (nm) ( $\pm 0.3$ )
1 h	24.6	$0.6 \times 10^{-3}$	0.003	0.015	5	20.1
10 h	18.3	$2.7 \times 10^{-3}$	0.007	0.022	3	16.1
20 h	11.1	$5.9 \times 10^{-3}$	0.013	0.032	2	14.7
30 h	10.8	$6.2 \times 10^{-3}$	0.021	0.074	4	13.4

**Table 3.2:** Microstructural parameters of Co ball milled with NiO powders, at 500 rpm, for different times in the weight ratio of 1:1.

Shown in figure 3.13 are the XRD patterns of 20 h ball milled Co+NiO, before annealing (a) and after annealing for 0.5 h and field cooling to room temperature ( $H = 5$  kOe) from two different temperatures, i.e. 600 K (curve (b)) and 740 K (curve (c)).

It can be observed in curve (b) that after annealing at  $T = 600$  K, NiO and Co peaks are not shifted in angle. However, there is a decrease of the peak width, due to a slight increase of the crystallite size. Moreover, after annealing at  $T = 600$  K Co powders are still basically in the hcp form. On the contrary, annealing at 740 K causes a certain amount of hcp-Co to allotropically transform into fcc. Moreover, annealing at higher temperatures, apart from inducing the hcp to fcc transformation, it also brings about a drastic increase of the crystallite size in the hcp phase. For example, from the  $(200)_H$  peak width, the crystallite size is found to increase from approximately 10 nm in the as-milled state to 18 nm after annealing at 740 K. It is also worth mentioning that annealing at  $T = 600$  K or 740 K does not result in formation of Co oxides, such as CoO or  $Co_3O_4$ .

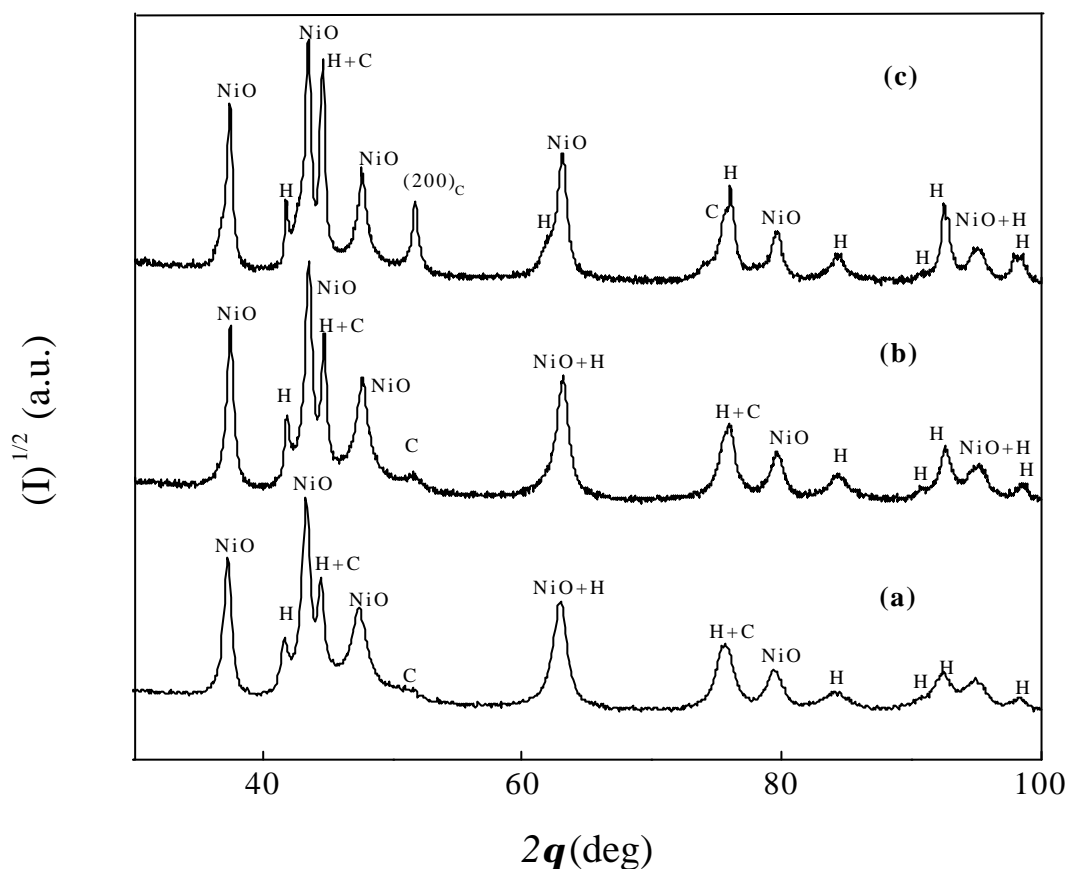


**Figure 3.13:** XRD patterns of 20 h ball milled Co + NiO, in a weight ratio of 1:1, before annealing (a) and after annealing and field cooling ( $H = 5$  kOe) from  $T = 600$  K (b) and  $T = 740$  K (c).

### **3.2.3.- The structural properties of SmCo<sub>5</sub> ball milled alone**

Contrary to ball milled Co, no phase changes are observed in SmCo<sub>5</sub> when it is subjected to ball milling. In addition, the amount of stacking faults accumulated during the milling of SmCo<sub>5</sub> particles is very small (e.g. ( $\mathbf{a}_{\text{SmCo}_5} + \mathbf{b}_{\text{SmCo}_5}$ )  $\sim 3 \times 10^{-3}$ ). The XRD patterns of SmCo<sub>5</sub> unmilled and milled for 1, 8 and 32 h are shown in figure 3.14. It can be seen that the milling process induces a broadening of the diffraction peaks, which is the result of crystallite size refinement and the increase of microstrains.

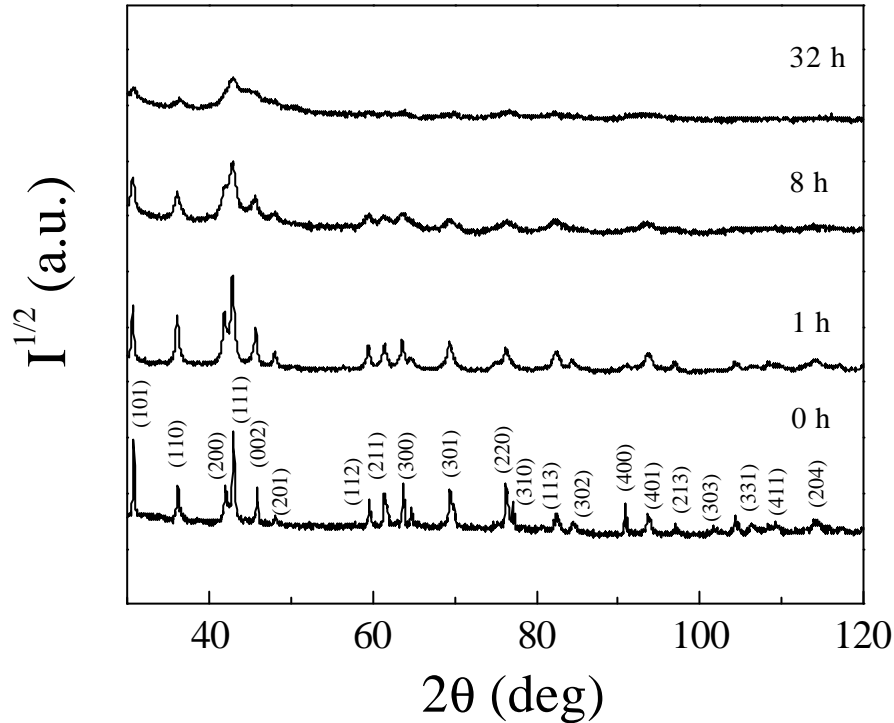


**Figure 3.14:** X-ray diffraction patterns of  $\text{SmCo}_5$  unground and ball milled for 1, 8 and 32 h. The Miller indexes of the main  $\text{SmCo}_5$  diffraction peaks are indicated in the figure.

The milling time dependences of  $\text{SmCo}_5$  crystallite size,  $\langle D \rangle_{\text{SmCo}_5}$  and microstrains,  $\langle \epsilon^2 \rangle^{1/2}$ , evaluated by means of the full-pattern fitting procedure (Rietveld method), are shown in figure 3.15. It is remarkable that after milling for 32 h,  $\langle D \rangle_{\text{SmCo}_5}$  is very small (smaller than 5 nm). This, together with the large microstrain values, is an indication that  $\text{SmCo}_5$  becomes close to amorphization after long-term milling. Similar results have been also reported by other authors [27,28].

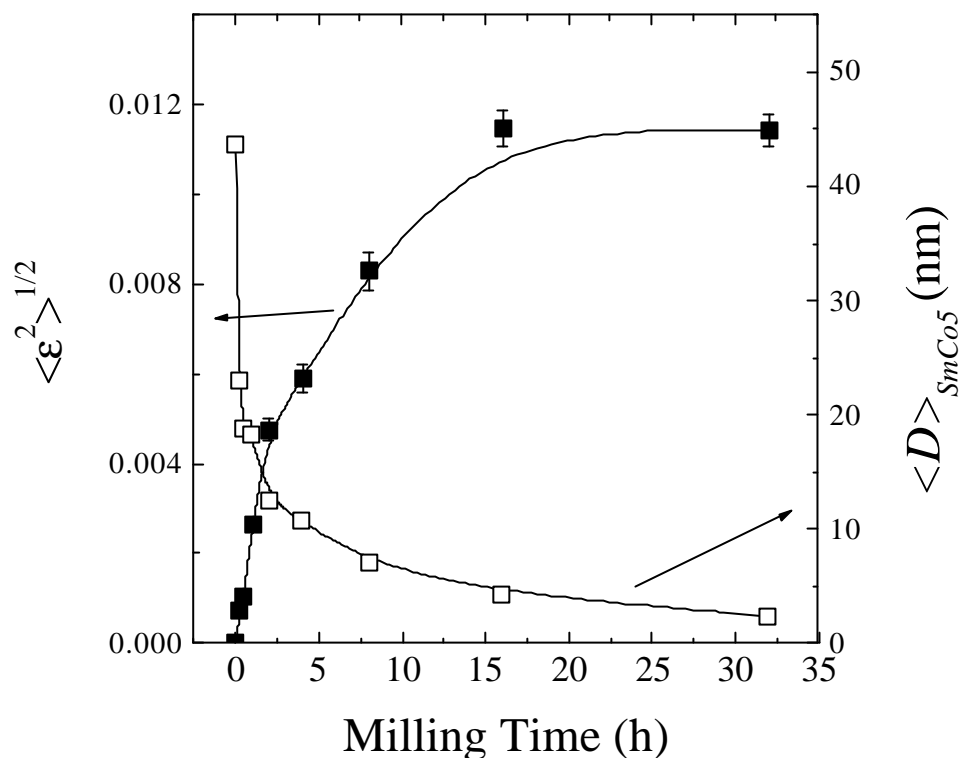


**Figure 3.15:** Milling time dependences of  $SmCo_5$  crystallite size,  $\langle D \rangle_{SmCo_5}$  (□), and microstrains,  $\langle \epsilon^2 \rangle^{1/2}$  (■). The error bars in  $\langle D \rangle_{SmCo_5}$  have not been plotted since they are smaller than the symbol sizes.

### 3.2.4.- The structural properties of $SmCo_5$ ball milled with NiO and with CoO

Shown in figure 3.16 are the XRD patterns of  $SmCo_5$  milled with NiO for 0.25, 4 and 32 h. Figure 3.17 shows the XRD pattern of  $SmCo_5$  milled with NiO for 16 h together with the fit obtained using the MAUD program (Rietveld method) and the difference between the experimental and calculated profiles.

As in  $SmCo_5$  milled alone, the stacking fault probability in  $SmCo_5$  ball milled with NiO is found to be very small (of the order of  $10^{-3}$ ), compared to ball milled Co (see figure 3.10). However, as in Co-NiO it can be observed that, for increasing milling times, the XRD peaks of both  $SmCo_5$  and NiO progressively broaden, indicating a reduction of the crystallite size and an increase of microstrains [3,4].

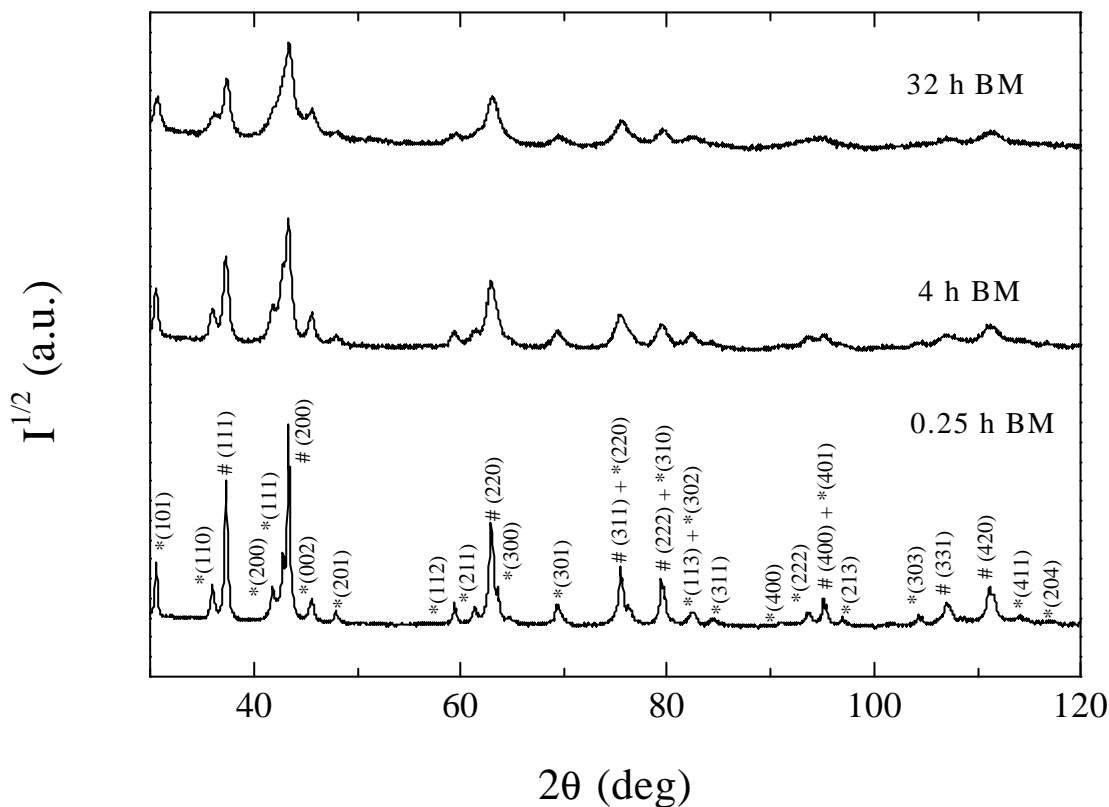


**Figure 3.16:** X-ray diffraction patterns of SmCo<sub>5</sub> + NiO ball milled during 0.25, 4 and 32 h, in the weight ratio 1:1. The symbols \* and # denote SmCo<sub>5</sub> and NiO peaks, respectively. Their Miller indexes are also indicated.

In figure 3.16 it can be seen that no other peaks, apart from those of SmCo<sub>5</sub> and NiO are generated during the milling. This indicates that no new phases are created during the milling. Moreover, since the position of the diffraction peaks remains virtually constant as the milling time increases, this points out that cell parameters do not vary with milling time, i.e. as for Co ball milled with NiO, there is not significant interdiffusion between SmCo<sub>5</sub> and NiO during the milling.

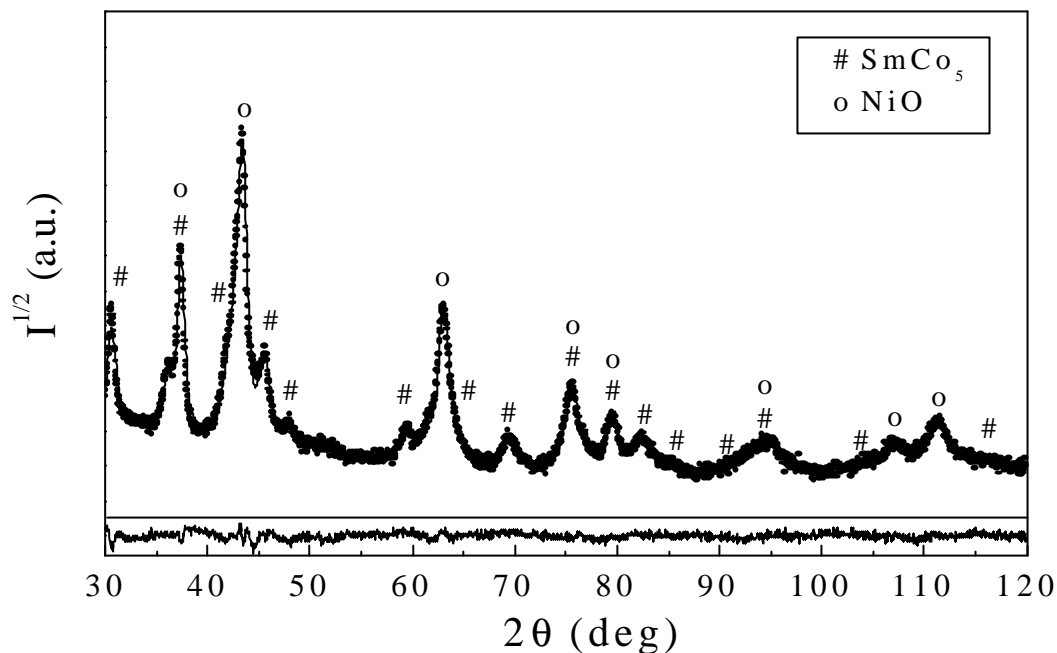


**Figure 3.17:** x-ray diffraction pattern of  $\text{SmCo}_5$  ball milled with NiO for 16 h in a weight ratio of 1:1, together with the curve generated from the full pattern fitting procedure and the corresponding difference between the calculated and the experimental profiles. The symbols # and o denote  $\text{SmCo}_5$  and NiO peaks, respectively.

Figure 3.18 shows the milling time dependence of the  $\text{SmCo}_5$  crystallite size,  $\langle D \rangle_{\text{SmCo}_5}$ , for several  $\text{SmCo}_5$ :NiO weight ratios. As can be seen in the figure, the reduction of crystallite size is rather steep for short milling times, although it tends to level off for longer milling times.

It can be seen also from figure 3.18 that, as the NiO content increases, the crystallite size reduction during the milling becomes smoother. It should be noted, for instance, that the crystallite size for  $\text{SmCo}_5$ , after long-term milling (e.g. 32 h), is much smaller when milled alone ( $\langle D \rangle_{\text{SmCo}_5} = 2.5$  nm) than when milled with NiO, i.e.  $\langle D \rangle_{\text{SmCo}_5} = 9$  nm for  $\text{SmCo}_5(1):(1)\text{NiO}$ .

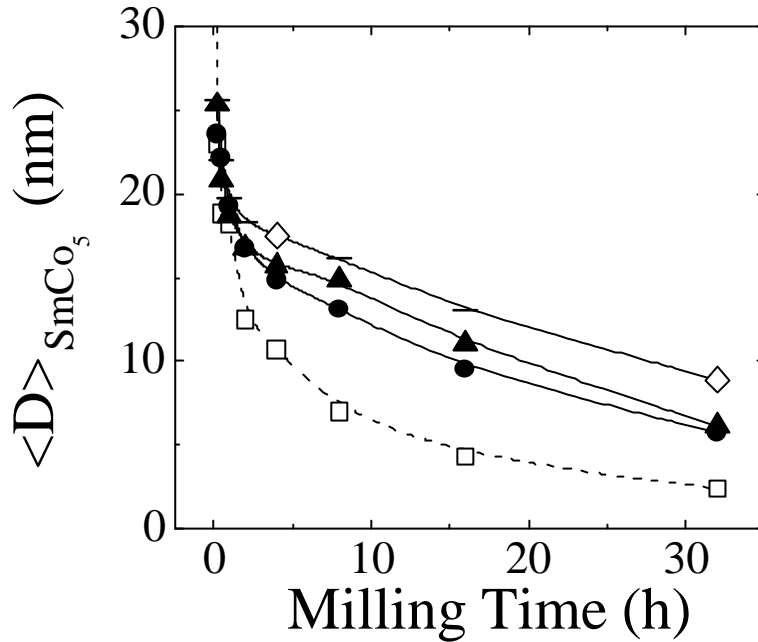


**Figure 3.18:** Milling time dependence of the  $\text{SmCo}_5$  crystallite size,  $\langle D \rangle_{\text{SmCo}_5}$ , for the  $\text{SmCo}_5$ :NiO weight ratios 1:0 (— □ —), 3:1 (— ● —), 3:2 (— ▲ —) and 1:1 (— ◇ —). Note that, for clarity, the crystallite size of the starting  $\text{SmCo}_5$  powders ( $\langle D \rangle_{\text{SmCo}_5, \text{initial}} = 43.4$  nm) has not been plotted. The error bars are not plotted since they are smaller than the symbol sizes.

The XRD patterns of  $\text{SmCo}_5$  ball milled with CoO for 0.25, 4 and 32 h can be seen in figure 3.19. As for  $\text{SmCo}_5$  milled with NiO, no extra-phases are created during the milling. Moreover, the amount of atomic interdiffusion between  $\text{SmCo}_5$  and CoO is also rather small, since the position of the diffraction peaks is found to remain unchanged as the milling proceeds.

Actually, the structural parameters of  $\text{SmCo}_5 + \text{NiO}$  and  $\text{SmCo}_5 + \text{CoO}$  composites are found to be very similar. Figure 3.20 shows the milling time dependences of  $\text{SmCo}_5$  crystallites size,  $\langle D \rangle_{\text{SmCo}_5}$ , for  $\text{SmCo}_5$  milled alone, with NiO and with CoO in the weight ratio 1:1. It can be seen in figure 3.20 that the evolution of  $\langle D \rangle_{\text{SmCo}_5}$  with milling time is rather similar for  $\text{SmCo}_5 + \text{NiO}$  and  $\text{SmCo}_5 + \text{CoO}$ , where for both systems  $\langle D \rangle_{\text{SmCo}_5}$  stabilizes at  $\langle D \rangle_{\text{SmCo}_5} \sim 10$  nm after long-term milling. This is an indication that similar to

SmCo<sub>5</sub> + NiO, milling with CoO also slows down SmCo<sub>5</sub> structural changes occurring during the milling process.

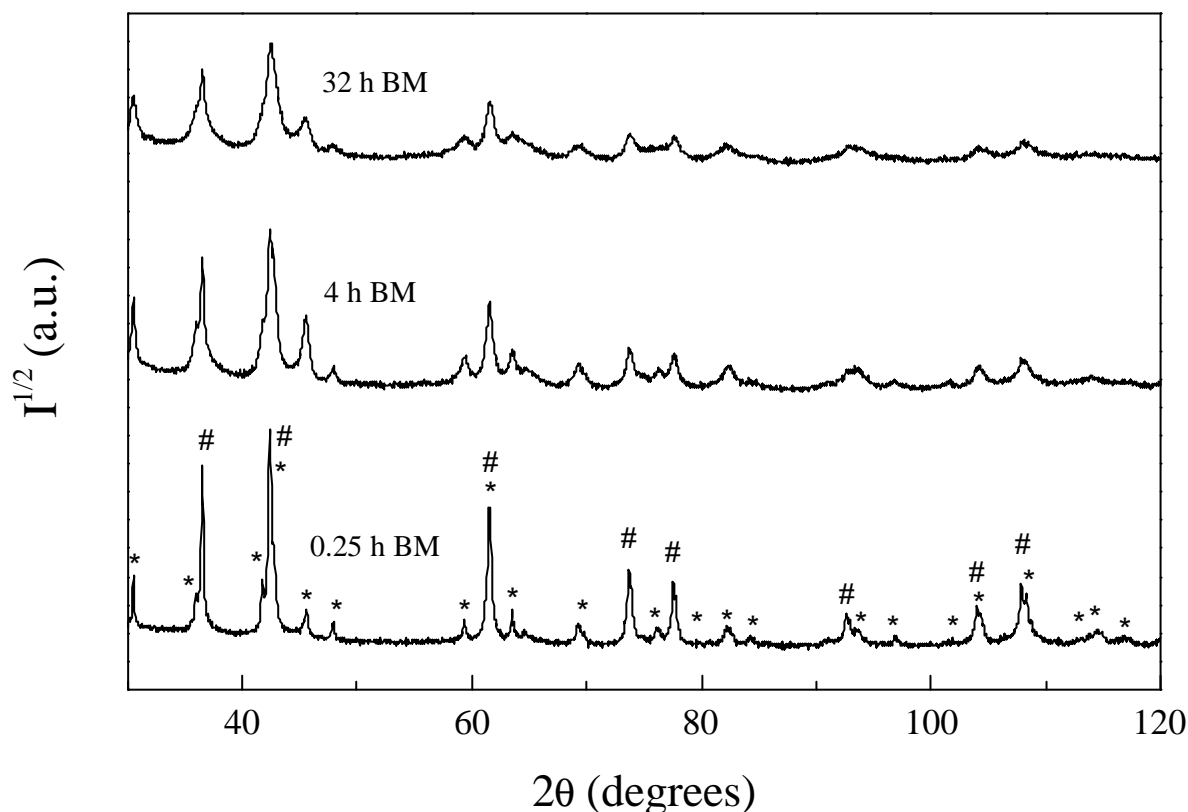


**Figure 3.19:** X-ray diffraction patterns of SmCo<sub>5</sub> + CoO ball milled during 0.25, 4 and 32 h, in the weight ratio 1:1. The symbols \* and # denote SmCo<sub>5</sub> and CoO peaks, respectively.

In addition, the microstrains,  $\langle \epsilon^2 \rangle^{1/2}$ , also increase with milling time in the three systems and, after long-term milling,  $\langle \epsilon^2 \rangle^{1/2}$  is found to be slightly larger in SmCo<sub>5</sub> than for SmCo<sub>5</sub> + NiO or SmCo<sub>5</sub> + CoO. This can be seen in figure 3.21. This is an indication that large amounts of structural defects, such as dislocations or vacancies, are introduced in the material during the milling. The small crystallite size and the large microstrain for SmCo<sub>5</sub> milled alone suggest that after 32 h SmCo<sub>5</sub> tends to amorphize. Nevertheless, as in the case

of Co + NiO, the milling appears to be less aggressive when SmCo<sub>5</sub> is milled with NiO or with CoO [3,4].

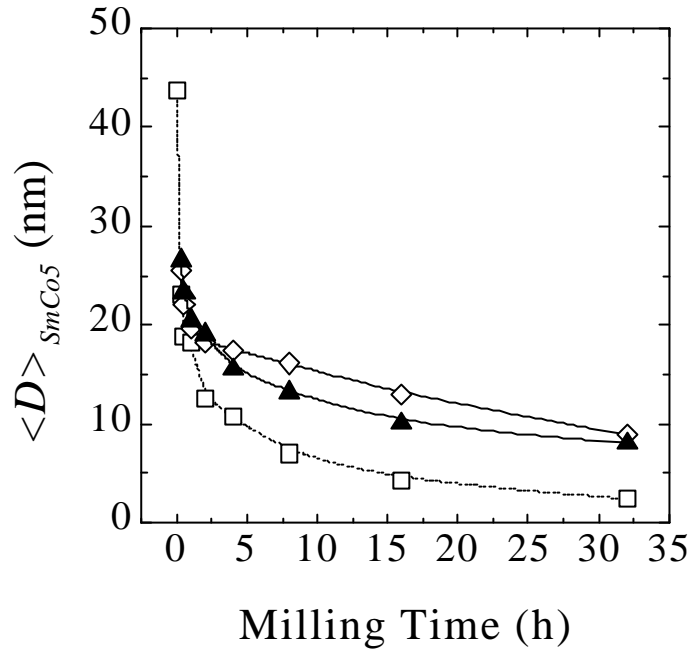


**Figure 3.20:** Milling time dependence of the SmCo<sub>5</sub> crystallite size,  $\langle D \rangle_{SmCo5}$ , for SmCo<sub>5</sub> milled alone (— □ —) and with NiO (— ◇ —) and CoO (— ▲ —) in the weight ratio 1:1. Note that the error bars are smaller than the symbol sizes.

It is noteworthy that the structural parameters and the morphology of as-milled SmCo<sub>5</sub> + CoO and SmCo<sub>5</sub> + NiO powders are very similar. In chapter 4 it will be shown that, in spite of these structural and morphological similarities, the two systems display very different magnetic behaviors when subjected to ball milling.

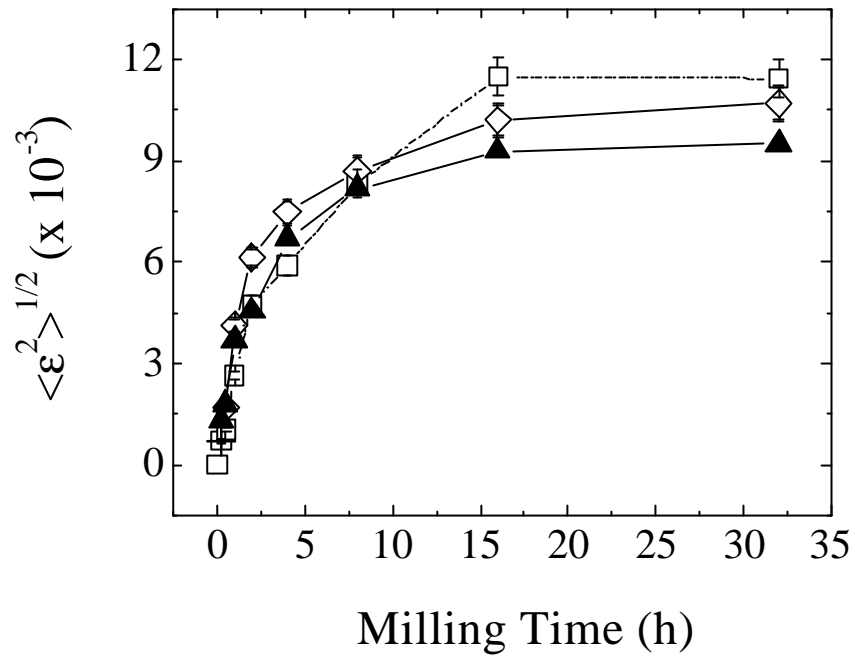


**Figure 3.21:** Milling time dependence of the microstrains in SmCo<sub>5</sub> structure,  $\langle \epsilon^2 \rangle^{1/2}$ , for SmCo<sub>5</sub> milled alone (--- □ ---) and with NiO (— ◇ —) and CoO (— ▲ —) in the weight ratio 1:1. The lines are a guide to the eye.

## References

- [1] J. Sort, J. Nogués, X. Amils, S. Suriñach, J.S. Muñoz, M.D. Baró, *Mat. Sci. Forum* **343-346** (2000) 812.
- [2] J. Sort, J. Nogués, X. Amils, S. Suriñach, J.S. Muñoz, M.D. Baró, *Mat. Res. Soc. Symp. Proc.* **581** (2000) 641.
- [3] J. Sort, J. Nogués, S. Suriñach, J.S. Muñoz, E. Chappel, F. Dupont, G. Chouteau, M.D. Baró, *Mat. Sci. Forum* **386-388** (2002) 465.
- [4] J. Sort, S. Suriñach, J.S. Muñoz, M.D. Baró, J. Nogués, G. Chouteau, V. Skumryev, G.C. Hadjipanayis, *Phys. Rev. B* **65** (2002) 174420.
- [5] J. Sort, N.M. Mateescu, J. Nogués, S. Suriñach, M.D. Baró, *J. Metast. Nanocryst. Mater.* **12** (2002) 126.
- [6] J. Sort, J. Nogués, S. Suriñach, M.D. Baró, *Phil. Mag. A* (2002), submitted.
- [7] T. Klassen, R. Günther, B. Dickau, A. Bartels, R. Bormann, H. Mecking, *Mat. Sci. Forum* **269-272** (1998) 37.
- [8] R. W. Hertzberg, *Deformation and fracture mechanisms of engineering materials* (John-Wiley & Sons, New York, 1995).
- [9] A.R. Troiano, J.L. Tokich, *Trans. Am. Inst., Metall. Pet. Eng.* **175** (1948) 728.
- [10] A. Z. Seeger, *Metallkd.* **60** (1969) 322; S. Mahajan, M.L. Green, D. Brasen, *Metall. Trans. A* **8** (1977) 283.
- [11] F. Cardellini, G. Mazzone, *Philos. Mag. A* **67** (1993) 1289.
- [12] T.B. Massalski, *Binary alloy phase diagrams* (American society for metals, Metals Park, 1986).
- [13] J.Y. Huang, Y.K. Wu, H.Q. Ye, *Appl. Phys. Lett.* **66** (1995) 308. J.Y. Huang, Y.K. Wu, H.Q. Ye, *Acta Mater.* **44** (1996) 1201.
- [14] J.Y. Huang, Y.K. Wu, H.Q. Ye, *Appl. Phys. Lett.* **67** (1995) 1945.

- [15] PCPDFWIN, JCPDS-ICDD ©, 1997.
- [16] D.G. Morris, *Mechanical behaviour of nanostructured materials, Materials Science Foundations* (Trans. Tech. Publications, Winthertur, Switzerland, 1998).
- [17] B.E. Warren, *X-ray diffraction* (Addison-Wesley, Reading, Massachusetts, 1969).
- [18] D. Hull, D.J. Bacon, *Introduction to dislocations* (Butterworth-Heinemann, Oxford, 2001).
- [19] G.E. Dieter, *Mechanical metallurgy* (McGraw-Hill Book Company, London, 1988).
- [20] O. Kitakami, H. Sato, Y. Shimada, F. Sato, M. Tanaka, Phys. Rev. B **56** (1997) 13849; S. Ram, Mat. Sci. Eng. A **304-306** (2001) 923.
- [21] C.G. Granqvist, R.A. Buhrman, J. Appl. Phys. **47** (1976) 2200; O. Kitakami, T. Sakurai, Y. Miyashita, Y. Takeno, Y. Shimada, H. Takano, H. Awano, Y. Sugita, Jpn. J. Appl. Phys. **35** (1996) 1724.
- [22] B.S. Murty, S. Ranhanathan, Internat. Mater. Rev. **43** (1998) 101.
- [23] H.J. Fecht, E. Hellstern, Z. Fu, W.L. Johnson, Metall. Trans. **21A** (1990) 2333.
- [24] C. Hitznerberger, H.P. Karnthaler, A. Korner, Acta. Metall. **33** (1985) 1293.
- [25] P. Tolédano, G. Krexner, M. Prem, H.P. Weber, V. P. Dimitriev, Phys. Rev. B **64** (2001) 144104.
- [26] V.P. Dimitriev, S.B. Rochal, Y.M. Gufan, Phys. Rev. Lett. **62** (1989) 2495.
- [27] D. L. Leslie-Pelecky, E. M. Kirkpatrick, and R. L. Schalek, Nanostruct. Mater. **12** (1999) 887; D. L. Leslie-Pelecky and R. L. Schalek, Phys. Rev. B **59** (1999) 457.
- [28] K. J. Strnat and R. M. W. Strnat, J. Magn. Mater. **100** (1991) 38.

## **Annex 4**

### **Magnetic Characterization**

This annex will deal with the magnetic properties of the FM-AFM systems studied in this thesis. In the first part, the main results concerning the Co + NiO system will be presented, focusing on the influence of several processing parameters on the final properties of the composites. A second part is devoted to the magnetic properties of SmCo<sub>5</sub> + NiO and SmCo<sub>5</sub> + CoO composites. In all cases, in order to discern the magnetic properties due to FM-AFM coupling from those related with the milling-induced microstructural changes, a comparison is made with the magnetic properties of FM particles (Co or SmCo<sub>5</sub>) milled without the presence of the AFM.

#### **4.1.- Magnetic properties of Co ball milled with NiO**

##### **4.1.1.- Influence of milling time on the coercivity**

To demonstrate the existence of FM-AFM exchange interactions in ball milled and heat treated Co + NiO powders, a comparison of the magnetic properties of Co milled alone and with NiO has been carried out [1-4]. In this section the influence of the milling time on the coercivity of as-milled powders will be analyzed.

Figure 4.1 shows the milling time dependence of coercivity of Co powders, before annealing and after annealing at 600 K for 0.5 h and field cooling ( $H = 5$  kOe) to room temperature. It can be seen that  $H_C$  first increases with milling time, reaching a maximum after 1 h of milling and subsequently starts to decrease for longer milling times. The increase of  $H_C$  for short milling times is mainly attributed to the transformation of the starting mixture of hcp + fcc Co to an almost pure hcp phase, since hcp-Co has a higher magnetic anisotropy.

The decrease of  $H_C$  for longer milling times is probably related to the accumulation of a large amount of defects (basically stacking faults) in the hcp structure (see section 3.2) and the subsequent appearance of fcc crystallites, which are known to decrease the magnetocrystalline anisotropy of Co [5].

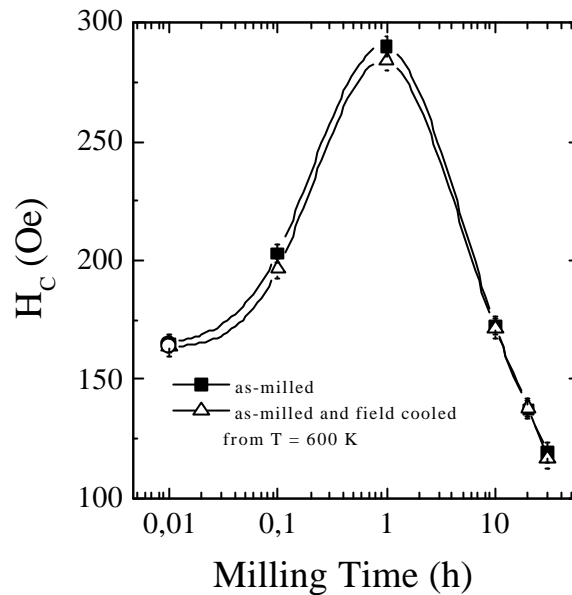


**Figure 4.1:** Milling time dependence of  $H_C$  (measured at room temperature) for Co powders, before annealing (-■-) and after annealing for 0.5 h at  $T = 600$  K and field cooling to room temperature ( $H = 5$  kOe) (-△-). Note that as-bought powders have been arbitrarily assigned to 0.01 h of milling.

The most remarkable aspect of figure 4.1 is that, after annealing and field cooling from  $T = 600$  K,  $H_C$  is virtually unchanged with respect to that of the as-milled powders. Only a slight decrease of  $H_C$  is observed, which can be understood in terms of crystallite size increase or a small transformation of hcp to fcc Co.

The magnetic behavior of Co milled with NiO is completely different. Shown in figure 4.2 is the milling time dependence of  $H_C$  for ball milled Co + NiO in a weight ratio of 1:1. As in the case of ball milled Co alone, a maximum is observed when plotting  $H_C$  as a function of milling time. However, in this case, the maximum appears after a longer milling time, i.e. 20 h, probably due to the role of NiO in slowing down Co structural changes during the milling, in particular the amount of stacking faults accumulated during the milling and the related transformation from hcp to fcc-Co (see section 3.2). It is noteworthy that the maximum  $H_C$  for ball milled Co + NiO is obtained precisely when the fcc-Co content in as-milled powders becomes minimum (see table 3.2).

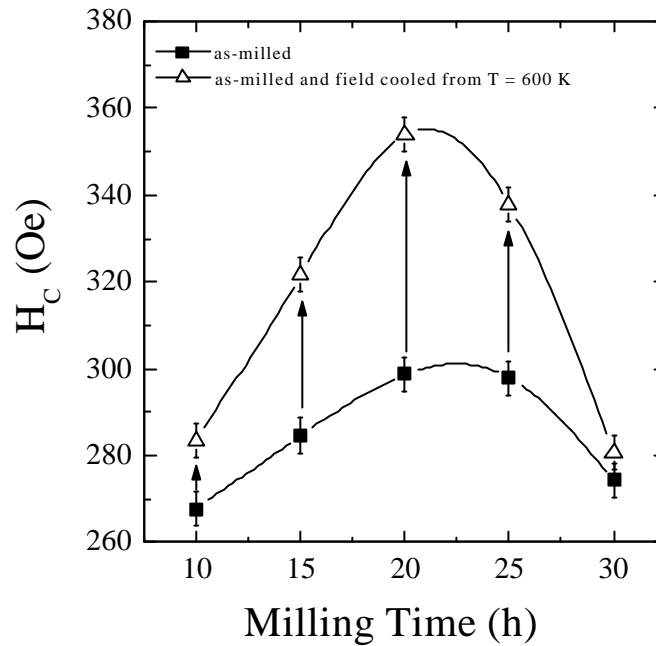


**Figure 4.2:** Milling time dependence of  $H_C$  (measured at room temperature) for ball milled Co + NiO powders (1:1 weight ratio), before annealing (-■-) and after annealing for 0.5 h at  $T = 600$  K and field cooling to room temperature ( $H = 5$  kOe) (-△-).

Moreover, contrary to Co ball milled alone, annealing for 0.5 h at  $T = 600$  K and field cooling to room temperature ( $H = 5$  kOe), results in a clear enhancement of  $H_C$ , for milling times longer than 10 h. This enhancement is around a 20 % compared to the maximum  $H_C$  of Co ball milled alone. Therefore, it is clear that NiO plays an important role in enhancing  $H_C$  of ball milled Co.

Shown in figure 4.3 is an enlargement of the hysteresis loops of Co ball milled with NiO, for 20 h, in a weight ratio of 1:1, before and after annealing at  $T = 600$  K, for 0.5 h and field cooling to room temperature applying a field  $H = 5$  kOe. It is remarkable that, after heat treatments, the hysteresis loop becomes broader and shifted along the field axis, although neither Co nor NiO experience significant structural changes during this process (see section 3.2.2). Thus, the  $H_C$  enhancement is mainly a magnetic and not a structural effect.

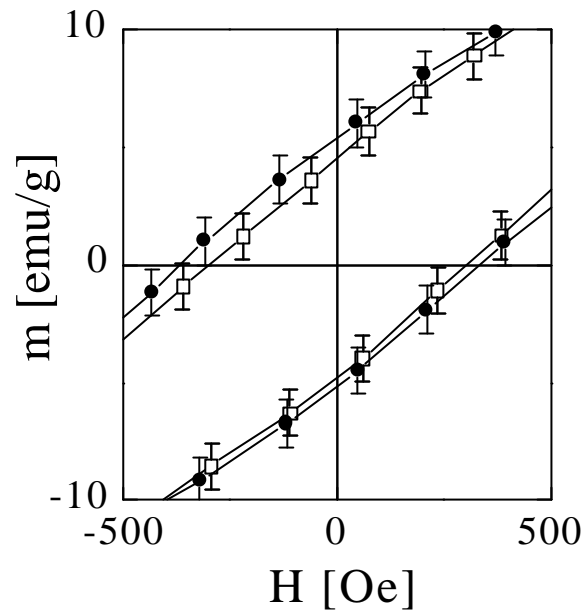


**Figure 4.3:** Enlargement of the hysteresis loops (measured at room temperature) for Co:NiO ball milled for 20 h in a weight ratio of 1:1, before (- □ -) and after (- ● -) annealing, under vacuum, at  $T = 600$  K, for 0.5 h, and cooling to room temperature applying a magnetic field  $H = 5$  kOe.

#### **4.1.2.- Influence of annealing temperature on coercivity, loop shift and squareness ratio**

In order to better understand the role of NiO in enhancing  $H_C$ , the 20 h ball milled Co + NiO powders have been annealed and field cooled from different temperatures,  $300 \text{ K} < T_{ANN} < 750 \text{ K}$ . The dependence of  $H_C$  on  $T_{ANN}$  is shown in figure 4.4. It is easily seen that  $H_C$  reaches a maximum value for  $T_{ANN} \sim 600 \text{ K}$ . This temperature is just above NiO Néel temperature,  $T_N = 590 \text{ K}$ . This is in agreement with the intuitive picture of FM-AFM coupling that has been reported in annex 1 and with many experimental results obtained in fine particles or in thin films (at room temperature or below) [6]. The fact that  $H_C$  is only enhanced for  $T_{ANN} > T_N$  is the first experimental evidence that FM-AFM exchange interactions may be induced between Co and NiO by means of ball milling and subsequent heat treatments. In contrast, annealing and field cooling ball milled Co powders (without the presence of AFM NiO) only results in a progressive decrease of  $H_C$  as  $T_{ANN}$  is increased.

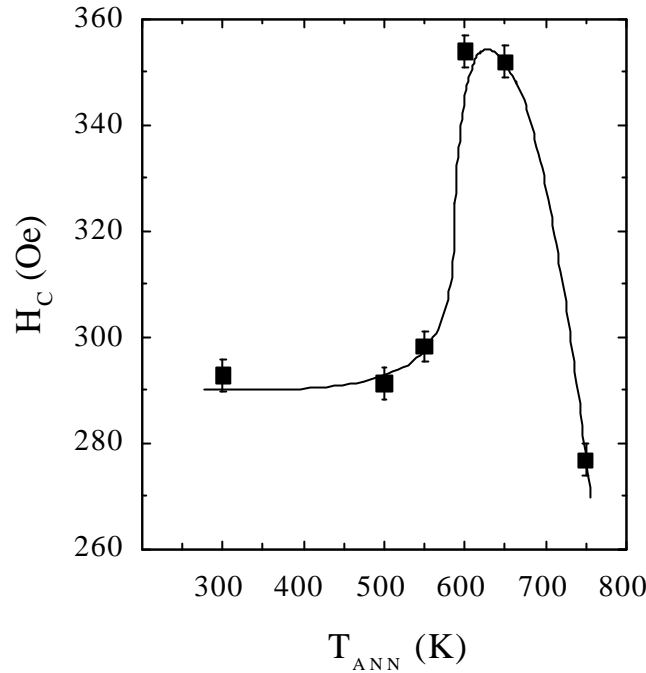


**Figure 4.4:** Dependence of  $H_C$  on the annealing temperature,  $T_{ANN}$ , for 20 h ball milled Co + NiO (in a weight ratio of 1:1). The as-milled powders were annealed for 0.5 h at  $T_{ANN}$  and subsequently field cooled ( $H = 5$  kOe) to room temperature.

In figure 4.4 it can also be seen that if  $T_{ANN}$  is higher than 650 K  $H_C$  is significantly reduced. This can be understood as a consequence of the allotropic phase transformation that occurs in Co (from hcp to fcc phase) when heated to above the transition temperature,  $T_t$ , which is usually around 700 K [7], although this temperature can be considerably lowered as the particle size is reduced [8].

Similar dependences of  $H_C$  on  $T_{ANN}$  have also been found in Co + NiO (weight ratio 1:1) for other milling times, as far as they are longer than 10 h, as seen in figure 4.5. This means that FM-AFM coupling can be already induced, to a certain extent, after milling for 10 h (and posterior field cooling) but not for shorter milling times, probably because the appropriate microstructure for the coupling, i.e. Co - NiO agglomerates with large amount of FM-AFM interfaces, requires a minimum of several hours of milling to be developed (see section 3.1).

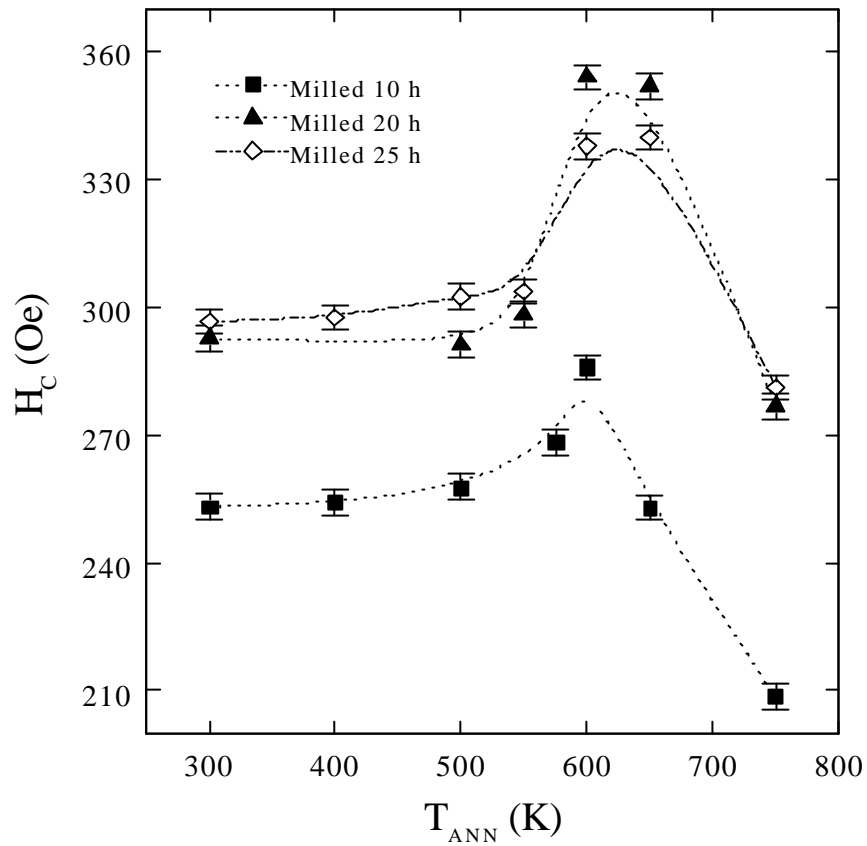


**Figure 4.5:** Dependence of  $H_C$  on the annealing temperature,  $T_{ANN}$ , for Co + NiO ball milled during 10, 20 and 25 h (in a weight ratio of 1:1). The as-milled powders were annealed for 0.5 h at  $T_{ANN}$  and subsequently field cooled ( $H = 5$  kOe) to room temperature.

Further evidence for these FM-AFM exchange interactions comes from the observation of shifted hysteresis loops (along the field axis), after field cooling from above  $T_N$  (NiO). The dependence of the loop shift,  $H_E$ , on  $T_{ANN}$  for 20 h ball milled Co + NiO is shown in figure 4.6.

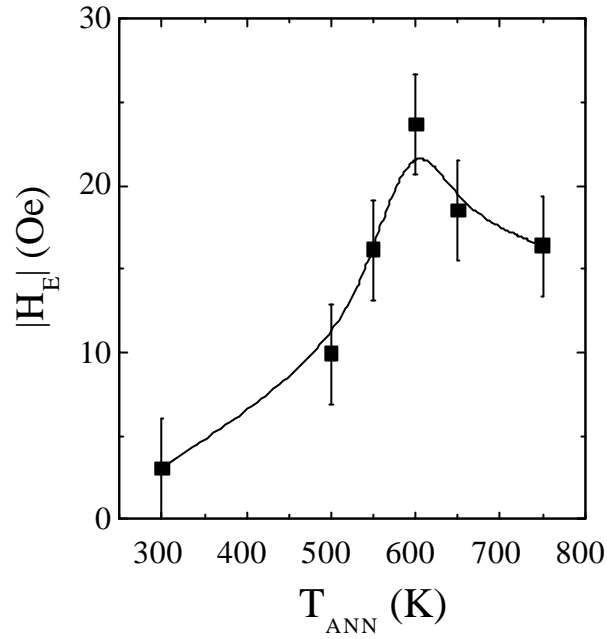


**Figure 4.6:** Dependence of  $H_E$  on the annealing temperature,  $T_{ANN}$ , for 20 h ball milled Co + NiO (in a weight ratio of 1:1). The as-milled powders were annealed for 0.5 h at  $T_{ANN}$  and subsequently field cooled ( $H = 5$  kOe) to room temperature.

The dependence of  $H_E$  on  $T_{ANN}$  is similar to that of  $H_C$ , i.e. a maximum is observed for  $T_{ANN} \approx T_N$ . Also noticeable is that for  $T_{ANN} < T_N$  small loop shifts are observed. In fact, due to thermal fluctuations, the AFM tends to magnetically disorder as temperature increases. Actually, the temperature at which FM-AFM exchange interactions effects disappear is sometimes lowered with respect to  $T_N$ , especially for very small AFM particles [9-12]. This is probably the reason for the observation of small loop shifts even for  $T_{ANN} < T_N$ . Moreover, in our case,  $H_E$  is found to be relatively small, compared to  $H_C$ . A similar result has been obtained in Ni-NiO fine powders [13] and Co-NiO thin films [14]. This is typical for systems in which the AFM anisotropy is relatively low (e.g.  $K_{NiO} < 5 \times 10^4$  erg/cm<sup>3</sup>) [6].

Besides the  $H_C$  enhancement, the squareness ratio,  $M_R/M_S$ , also increases in ball milled Co-NiO, compared to ball milled Co alone, after field cooling from  $T > T_N$ . Shown in figure 4.7 is the dependence of  $M_R/M_S$  on  $T_{ANN}$  for Co ball milled with NiO in a weight ratio of 1:1, during 20 h, and field cooled from  $T_{ANN}$  applying a magnetic field  $H = 5$  kOe. The dependence of  $M_R/M_S$  on  $T_{ANN}$  has been found to be similar to that of  $H_C$  or  $H_E$ , suggesting that, although the origin of the  $M_R/M_S$  enhancement still remains somewhat unclear, it can be related, at least in part, to the existence of FM-AFM interactions.

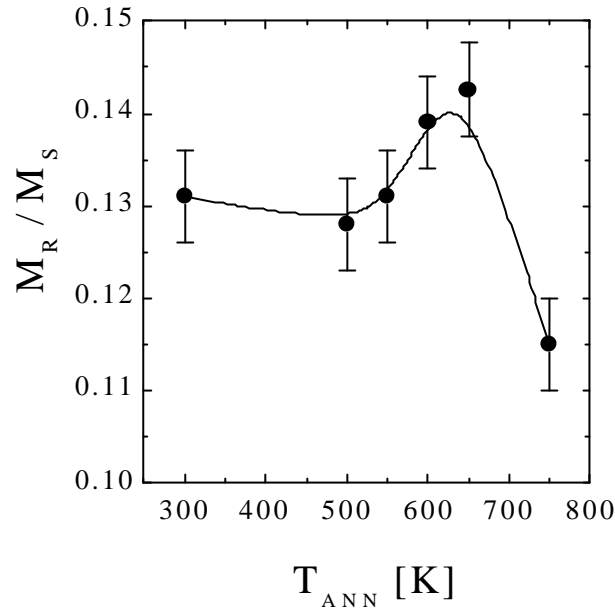


**Figure 4.7:** Dependence of  $M_R/M_S$  on the annealing temperature,  $T_{ANN}$ , for 20 h ball milled Co + NiO (in a weight ratio of 1:1). The as-milled powders were annealed for 0.5 h at  $T_{ANN}$  and subsequently field cooled ( $H = 5$  kOe) to room temperature.

It is noteworthy that  $M_R/M_S$  enhancements have been also occasionally observed in other FM-AFM systems [15]. However, although it is difficult to fully understand its origin, it is possible to draw an intuitive picture to figure out, at least qualitatively, how FM-AFM exchange interactions could contribute to the enhancement of  $M_R/M_S$ . A simplified model will be discussed in annex 5.

#### **4.1.3.- Influence of the cooling field strength on the coercivity enhancement and loop shift**

It is expected that, during field cooling experiments, the strength of FM-AFM coupling induced between Co and NiO would increase with the field applied during the cooling,  $H_{FC}$ . This should occur because the FM increases its overall magnetic moment under application of higher magnetic fields and, therefore, the spins of the AFM will better align with those in the FM, thus leading to an optimum coupling. However, once the saturation of the FM is reached, no further changes should take place. Figure 4.8 (a) shows the dependence

of the coercivity enhancement,  $\Delta H_C$  (difference of coercivity between after and before the field cooling procedure), on  $H_{FC}$  for Co milled with NiO for 20 h in the weight ratio of 1:1. Figure 4.8 (b) shows the dependence of  $|H_E|$  on  $H_{FC}$ . It can be seen that, as expected, both  $\Delta H_C$  and  $|H_E|$  increase with  $H_{FC}$  for cooling fields lower than 5 kOe.

However, after a maximum, both  $\Delta H_C$  and  $|H_E|$  are found to decrease with  $H_{FC}$ . This anomalous behavior could be explained as due to a *spin-flop transition* in the AFM. It has been shown, both theoretically and experimentally, that when the magnetic field applied along the easy axis of an AFM single crystal, is large enough (i.e. above the so-called spin-flop field,  $H_{spin-flop}$ ) it is energetically favorable for the spins in the AFM to orient perpendicular to the magnetic field instead of parallel to it, i.e. the spins “flip” to a direction orthogonal to the magnetic field [16,17].

In the case of NiO, in the temperature range from room temperature to  $T_N$ ,  $H_{spin-flop}$  has been reported to be between 6 and 10 kOe [18]. Therefore, although in our case the AFM is not a single crystal, it is reasonable to think that the decrease of  $\Delta H_C$  and  $|H_E|$  might be related to the AFM spin-flop, since a fair amount of the AFM particles will be oriented in directions close to AFM easy axis of NiO. The effect of spin-flop on FM-AFM exchange coupling has been systematically studied in  $MnF_2$ -Fe thin films and, in particular, it has been shown to reduce the amount of loop shift [19].

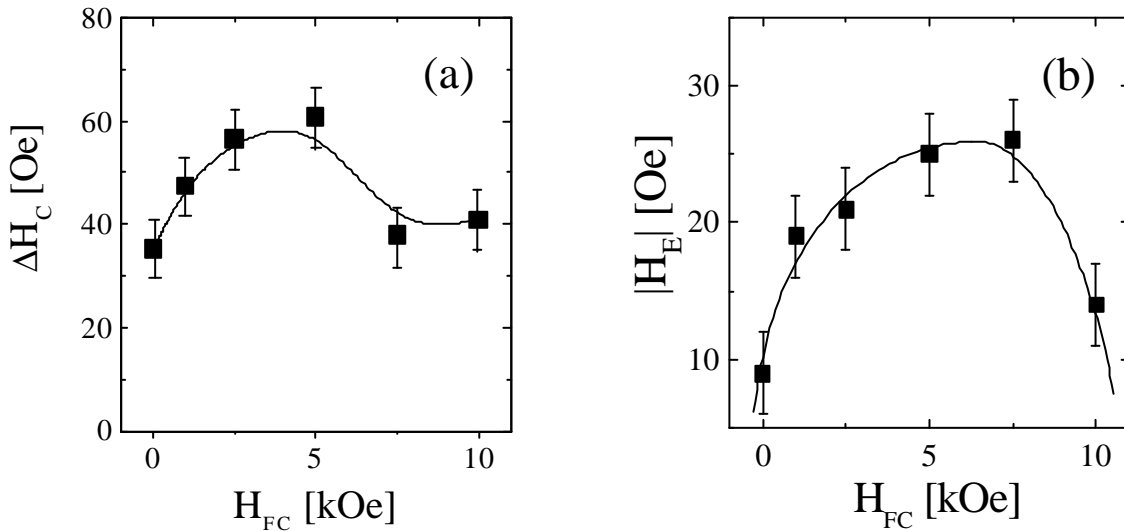


**Figure 4.8:** Dependence of the coercivity enhancement,  $\Delta H_C$ , and loop shift,  $|H_E|$ , on the magnetic field applied during field cooling experiments,  $H_{FC}$ , for Co ball milled with NiO for 20 h in the 1:1 weight ratio.

Figure 4.8 also shows that the effects of the coupling, e.g. loop shift and coercivity enhancement, appear even after cooling in zero applied field. The appearance of FM-AFM exchange interactions after zero field cooling can be understood as a result of the remanent magnetization existing in Co during the cooling experiment. Nevertheless, as shown in the figure, the maximum values of  $\mathbf{DH}_C$  and  $|H_E|$  are encountered for  $H_{FC} = 5$  kOe. Therefore, this field has been chosen to carry out most of our experiments.

#### **4.1.4.- Influence of the FM:AFM weight percentages on the coercivity and energy product enhancements**

The FM:AFM weight ratio has also been varied in order to try to further increase  $H_C$  and to analyze the effect of composition on the energy product of the composites [2]. Therefore, a new batch of samples was prepared, choosing FM:AFM ratios of 1:0, 7:3, 3:2, 1:1 and 2:3. For all compositions,  $H_C$  is found to first increase with the milling time and then progressively decrease, due to the structural changes occurring in Co when subjected to ball milling. The milling time dependences of  $H_C$ , measured at room temperature, for the FM:AFM weight ratios of 3:2 and 1:1, before and after annealing at  $T_{ANN} = 600$  K and field cooling ( $H = 5$  kOe) to room temperature are shown in figure 4.9. It is found that the milling time corresponding to maximum  $H_C$  in each case,  $t_{Max}$ , is found to shift towards higher values as the NiO content increases. This is mainly due to the role of NiO in slowing down Co structural changes during the milling. Moreover, after field cooling from above  $T_N$ , an enhancement of  $H_C$  is observed for both compositions, due to the induction of FM-AFM exchange interactions.

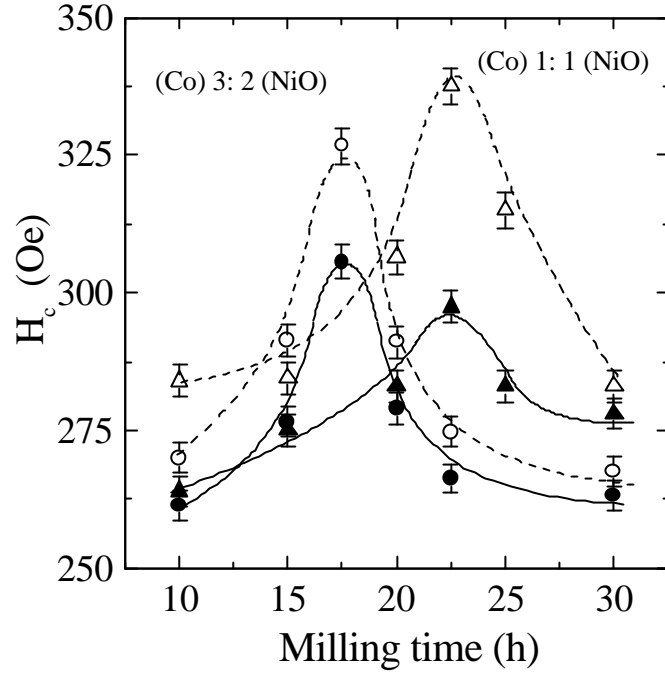


**Figure 4.9:** Milling time dependence of the coercivity,  $H_C$ , measured at room temperature, for Co ball milled with NiO in the weight ratios 3:2 (--○--) and 1:1 (--△--). The filled symbols correspond to as-milled powders (before annealing), while open symbols correspond to powders annealed at  $T = 600$  K for 0.5 h and field cooled ( $H = 5$  kOe) to room temperature.

A summary of the magnetic properties of ball milled Co + NiO, for different compositions, before and after field cooling ( $H_{FC} = 5$  kOe), is given in table 4.1. Apart from  $t_{Max}$ ,  $H_C$  (before and after F.C. from  $T_{ANN} = 600$  K) and  $H_E$  (after F.C.), also the values of coercivity enhancement,  $\mathbf{DH}_C = H_C$  (after F.C.)  $- H_C$  (before F.C.) and the energy product,  $(BH)_{Max}$  (after F.C.), corresponding to  $t_{Max}$ , are shown in table 4.1 as a function of the FM:AFM percentages.

From the table it is clear that, for all compositions, except for pure Co, an enhancement of  $H_C$  and a loop shift are observed after annealing and field cooling from  $T_{ANN} = 600$  K. The maximum  $\mathbf{DH}_C$  and  $H_E$  are obtained for the FM:AFM ratio of 1:1.

% (weight) Co	$t_{Max}$ (h)	$H_C(t_{Max})$ ( $\pm 10$ Oe) [before FC]	$H_C(t_{Max})$ ( $\pm 10$ Oe) [after FC]	$\mathbf{DH}_C(t_{Max})$ ( $\pm 7$ Oe)	$ H_E (t_{Max})$ ( $\pm 7$ Oe) [after FC]	$(BH)_{Max}(t_{Max})$ (G.Oe $\cdot 10^4$ ) [after FC]
100 (1:0)	1	288	284	-4	2	$7.1 \pm 0.7$
70 (7:3)	12.5	280	309	29	8	$7.6 \pm 0.7$
60 (3:2)	17.5	302	330	28	10	$8.3 \pm 0.7$
50 (1:1)	22.5	297	344	47	22	$6.2 \pm 0.6$
40 (2:3)	25	264	280	16	8	$2.9 \pm 0.5$

**Table 4.1:** Summary of the magnetic properties of ball milled Co + NiO, measured at room temperature, for different FM:AFM weight ratios, where  $t_{Max}$  is the milling time corresponding to the maximum  $\mathbf{DH}_C$  in each composition. All values of  $H_C$ ,  $|H_E|$  and  $(BH)_{Max}$  are given for  $t_{Max}$ .

As mentioned in annex 1, the magnitude that determines the quality of a permanent magnet is the maximum energy product,  $(BH)_{Max}$  [20]. Shown in figure 4.10 is the dependence of  $(BH)_{Max}$  on the NiO content, after milling during  $t_{Max}$ , before and after annealing the as-milled powders for 0.5 h at  $T_{ANN} = 600$  K and field cooling to room temperature ( $H = 5$  kOe). In the as-milled state,  $(BH)_{Max}$  tends to decrease as the NiO content increases, essentially because of the decrease of the overall  $M_S$ , due to the zero net magnetization of the AFM. Nevertheless, after field cooling the powders, one observes for all compositions (except for pure Co) an enhancement of  $(BH)_{Max}$ , mainly due to the enhancements of  $H_C$  and  $M_R/M_S$  resulting from the FM-AFM exchange interactions. It is noteworthy that, although the maximum  $H_C$  enhancement is obtained for the weight ratio 1:1,  $(BH)_{Max}$  is further enhanced for the FM(3):(2)AFM ratio. This is because of the two-fold role of the AFM. On the one hand, higher NiO contents bring about a higher  $(BH)_{Max}$  because of the increase of FM-AFM interactions. On the other hand, if the AFM content is increasingly high, the effects of the coupling are not enough to overcome the reduction of  $M_S$  due to the AFM and, thus,  $(BH)_{Max}$  is not enhanced [2].

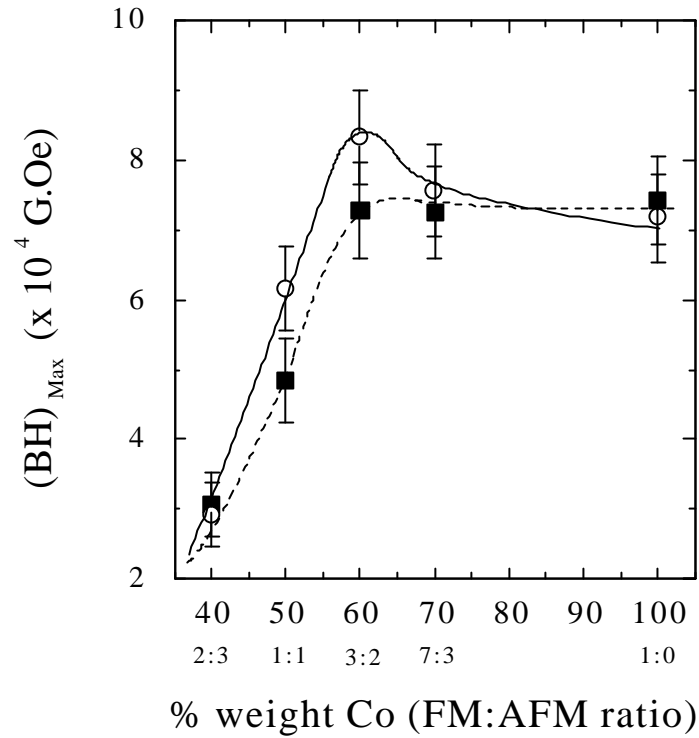


**Figure 4.10:** Dependence of the energy product,  $(BH)_{Max}$  (measured at room temperature), on the NiO content, before (-■-) and after (-○-) annealing for 0.5 h at  $T_{ANN} = 600$  K and field cooling ( $H = 5$  kOe) to room temperature.

#### 4.1.5.- Thermal dependence of the coercivity enhancement, the loop shift and the energy product enhancement

Since the coupling depends on the spin configurations at the interfaces between the FM and AFM components, it is reasonable to assume that thermal energy will play an important role on the coupling between them. Namely, the effects of coupling will tend to decrease as temperature is increased, because of the loss of magnetic order in the FM and AFM materials. In the preceding sections, all presented results correspond to measurements performed at room temperature. To analyze the effect of temperature on the exchange-coupled composites, the following procedure has been carried out:

- Co has been ball milled with NiO for 20 h in a weight ratio of 1:1.
- The as-milled powders have been annealed at  $T_{ANN} = 600$  K, for 0.5 h.

- A field cooling process ( $H = 5$  kOe) to room temperature has been carried out, in order to induce FM-AFM exchange interactions.
- Once the coupling is induced, the powders have been heated again and hysteresis loops have been measured at different temperatures above room temperature, in order to study the thermal stability of exchange coupled FM-AFM composites.

Shown in figure 4.11 are the thermal dependences of  $\Delta H_C$ ,  $|H_E|$  and  $\Delta(BH)_{Max}$ , where  $\Delta(BH)_{Max}$  is defined as  $(BH)_{Max}$  (after annealing) –  $(BH)_{Max}$  (before annealing). Note that  $\Delta H_C$  has already been defined also as the difference of coercivities between after and before the field cooling processes.

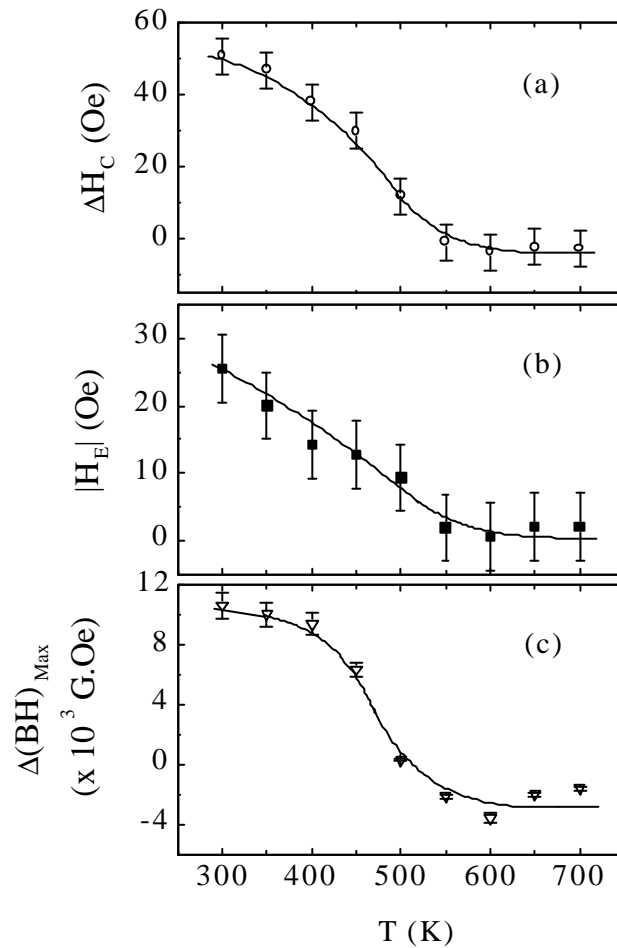


**Figure 4.11:** Thermal dependences of (a) coercivity enhancement,  $\Delta H_C$ , (b) loop shift,  $|H_E|$ , and (c) enhancement of the energy product,  $\Delta(BH)_{Max}$ , of Co ball milled with NiO for 20 h, in the weight ratio of 1:1, measured all of them at the temperature T. Note that  $\Delta H_C$  and  $\Delta(BH)_{Max}$  have been obtained by taking the difference of  $H_C$  and  $(BH)_{Max}$ , between after and before annealing for 0.5 h at  $T_{ANN} = 600$  K and field cooling to room temperature ( $H = 5$  kOe). The lines are a guide to the eye.

It can be seen from figure 4.11 that the three parameters ( $DH_C$ ,  $|H_E|$  and  $D(BH)_{Max}$ ) progressively decrease as temperature is increased, vanishing almost completely for  $T \geq 600$  K. This is the typical behavior for FM-AFM exchange coupled systems: the coupling decreases with temperature because of the loss of magnetic order in the AFM and the decrease of AFM magnetocrystalline anisotropy [6]. As has been described in the introduction, in order to induce a loop shift the following condition has to be fulfilled:  $K_{AFM} \cdot t_{AFM} > J_{INT}$ . Upon heating,  $K_{AFM}$  is progressively reduced and above a certain temperature, called *blocking temperature*,  $T_B$ , this inequality is no longer accomplished and, therefore, the loop shift is no longer observed. Usually  $T_B$  is close or equal to  $T_N$  [9-12]. The fact that in many systems  $T_B < T_N$  is related, at least in part, to reduced AFM crystallite sizes or too thin AFM layers. If the AFM crystallites are exceedingly small, due to finite size effects, the ordering temperature in the AFM becomes significantly reduced [11,12,21]. However, in our case, loop shifts are observed for temperatures up to  $T_N$ , i.e.  $T_B \sim T_N$ .

Nevertheless, it should be noted that, according to Meiklejohn and Bean's model, the decrease of the AFM anisotropy should bring about an increase of coercivity when, during the heating, the condition  $K_{AFM} \cdot t_{AFM} > J_{INT}$  is no longer fulfilled [22]. In fact, in some systems, a peak in  $H_C$  has been observed for temperatures close to  $T_B$  [23-25]. However, in general, this peak in  $H_C$  is not observable because usually there is a distribution of blocking temperatures. Several authors have suggested that in an exchange coupled FM-AFM material there exist several "exchange paths", each of them having its own unidirectional magnetic anisotropy and local blocking temperature,  $T_{Bi}$  [10,26,27]. In other words, one can think of the material to be composed of several zones, where, upon heating, the coupling in each of them disappears at different temperatures,  $T_{Bi}$ . Thus, each zone should have a peak in  $H_C$  at a different temperature and due to the distribution of grain sizes, defects or anisotropies, the effect is averaged out. The temperature at which the coupling disappears completely is therefore what is designated as blocking temperature, i.e.  $T_B$  corresponds to the maximum value of  $T_{Bi}$ .

#### **4.1.6.- Thermal stability of the FM:AFM coupling**

The existence of a  $T_{Bi}$  distribution can affect the thermal stability of the exchange-coupled material, since for regions with  $T_{Bi}$  close to room temperature the effects of the coupling will rapidly disappear with slight increments of temperature. In order to evaluate the thermal stability of the exchange-coupled composites (i.e. the degree of coupling still

remaining after heating to a certain temperature) the following experimental procedure was carried out [4]:

- First, Co and NiO were milled together during 20 h in the weight ratio 1:1.
- The as-milled powders were subsequently annealed for 0.5 h at  $T_{ANN} = 600$  K and field cooled ( $H = 5$  kOe) to room temperature in order to induce the exchange coupling between Co and NiO.
- A hysteresis loop was performed at room temperature.
- Then, the powders were heated again up to a certain temperature,  $T_D$  ( $T_D > RT$ ). It was assumed that during this second heating part of the coupling induced by the previous field cooling procedure would disappear.
- A hysteresis loop was carried out at  $T_D$  and it was checked that, effectively, the effects of the coupling ( $H_E$ ,  $\mathbf{DH}_C$  and  $\mathbf{D(BH)}_{Max}$ ) were reduced due to the heating.
- After the hysteresis loop, at  $T = T_D$ , the magnetic field was switched to a negative polarity ( $H = - 5$  kOe) and the sample was field cooled in the negative field to room temperature.
- Another hysteresis loop was carried out at room temperature to observe the effect of having certain FM-AFM regions of the material exchange coupled applying a positive field (first field cooling) and others exchange coupled applying a negative field (second field cooling).

This procedure was repeated varying  $T_D$  from room temperature to  $T = 700$  K.

The results of this experiment are shown in figure 4.12. The figure illustrates the dependence of  $H_E$  on the temperature of measurement (after the first field cooling, i.e. when the coupling is induced) and, also the values of  $H_E$  obtained at room temperature after the second field cooling, i.e. applying a negative cooling field. From these measurements it is possible to have an idea of the distribution of blocking temperatures on the exchange coupled FM-AFM system.

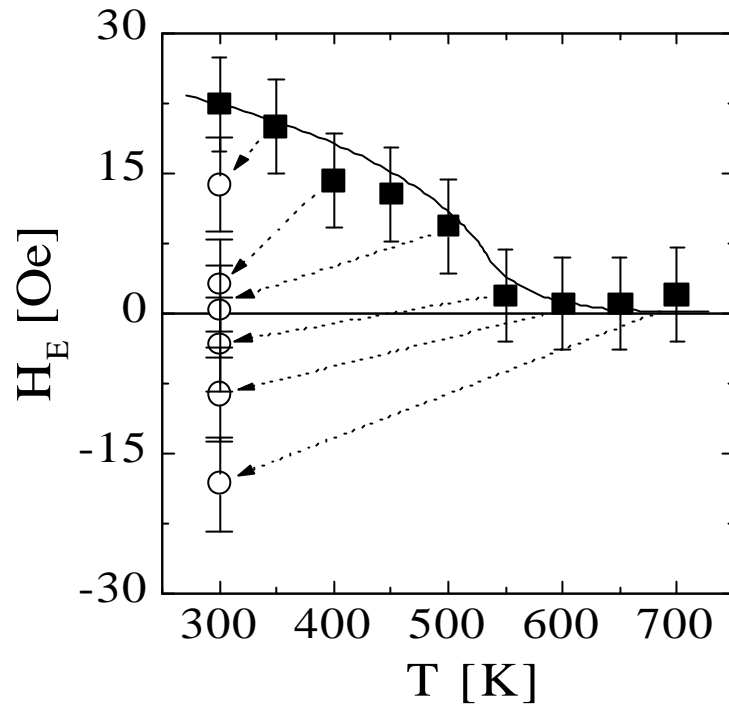


**Fig. 4.12:** Temperature dependence of the exchange bias,  $H_E$ , on the measuring temperature ( $\blacksquare$ ), and values of  $H_E$ , measured at room temperature ( $\circ$ ), after field cooling in  $H = -5$  kOe from different temperatures.

Following this procedure, when the sample is heated to  $T = T_D$ , all AFM grains with  $T_{Bi}$  lower than  $T_D$  will become magnetically disordered, therefore losing the information of their original coupling, while the grains with  $T_{Bi} > T_D$  will still remain exchange coupled. If regions with  $T_{Bi} < T_D$  are field cooled applying  $H = -5$  kOe FM-AFM exchange coupling will be induced in them in opposite sense to the original coupling. This is schematically shown in figure 4.13, where the AFM domains are represented as vertical cylinders. Note that the regions with  $T_{Bi} < T_D$  will contribute to shift the hysteresis loop towards the positive field axis instead of towards the negative field axis (as it was in the coupling originated during the first field cooling experiment).

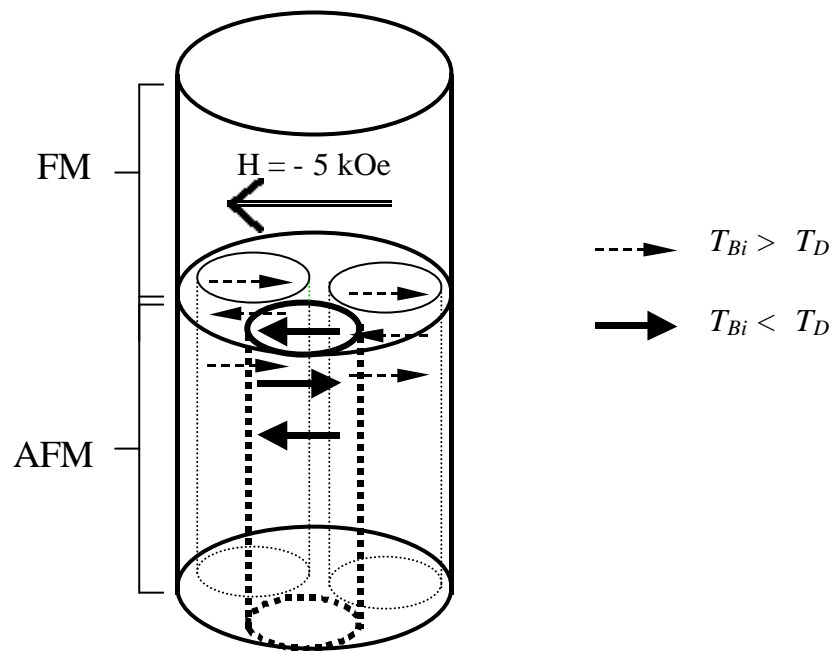


**Figure 4.13:** Schematic diagram of the spin configuration in the AFM, after the second field cooling procedure, using a negative magnetic field ( $H = -5$  kOe). Note that only those AFM regions with  $T_{Bi} < T_D$  are shifted during the second field cooling, while those with  $T_{Bi} > T_D$  remain oriented in the direction of the first field cooling (using  $H = 5$  kOe)

Note that if  $T_B$  was univocally defined, for  $T_D < T_B$  one would always obtain, after the second field cooling, the same value of  $H_E$  at room temperature as after the first field cooling, e.g.  $H_E = 22$  Oe, since the second heat treatment would not be able to erase the effects of the first coupling. Conversely, for  $T_D > T_B$  one would always obtain  $H_E = -22$  Oe, since all the FM-AFM crystallites would then become uncoupled at  $T_D$  and a shift towards the opposite direction would be induced during the second field cooling. As can be seen in figure 4.12, already at  $T_D = 350$  K a reduction in  $H_E$  can be observed. Moreover, for  $T_D = 500$  K  $H_E$  is reduced to zero after the second field cooling experiment (i.e. 50 % of the crystallites have  $T_{Bi} < 500$  K). These results indicate there is a broad distribution of blocking temperatures in this

system. A schematic picture of the local blocking temperature distribution is shown in figure 4.14.

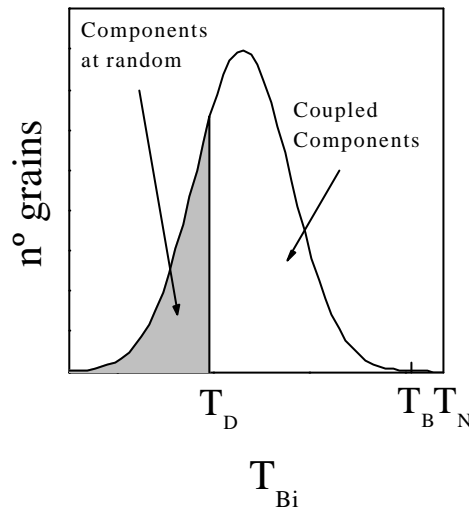


**Figure 4.14:** Schematic picture of the local blocking temperature distribution. Note that during the second heat treatment at a certain temperature  $T_D$ , those grains with  $T_{Bi} < T_D$  are uncoupled during the heating, while the grains with  $T_{Bi} > T_D$  still remain coupled in the direction of the first field cooling procedure.

However, it should be noted that, although the thermal stability of  $H_E$  is strongly influenced by the distribution of  $T_{Bi}$ , it was observed that  $H_C$  is rather insensitive to it (e.g.  $H_C \sim 345$  Oe). This is probably because although the overall  $H_E$  depends on the strength and sign of the coupling for each crystallite, the enhancement of  $H_C$  depends only on the strength of the coupling, independently of field cooling with a negative or a positive magnetic field has induced it [4].

#### **4.1.7.- Comparison with the magnetic properties of the Co+FeS system**

It is interesting to mention that the same processing route than in Co + NiO has also been applied to Co+FeS and some evidences of FM-AFM exchange interactions induced by ball milling (such as the presence of loop shifts or coercivity enhancements) have also been

observed [1]. For example, from the curve  $H_C$  vs.  $T_{ANN}$  (for 10 h ball milled Co+FeS in a weight ratio of 1:1), a maximum in  $H_C$  has also been observed at  $T_{ANN} = 650$  K (see figure 4.15). The fact that the maximum appears at  $T_{ANN} = 650$  K (and not at  $T_{ANN} = 600$  K, like in Co-NiO, see figure 4.5) is attributed to the difference in Néel temperatures between NiO and FeS, i.e.  $T_N$  (NiO) = 590 K, while  $T_N$  (FeS) = 613 K. Therefore,  $H_C$  is only enhanced after field cooling from above  $T_N$  (FeS), as expected from FM-AFM exchange coupling.

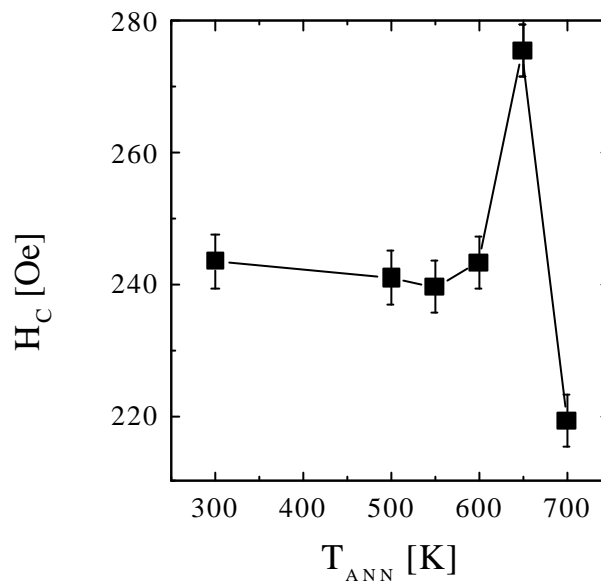


**Figure 4.15:** Dependence of  $H_C$ , measured at room temperature, on the annealing temperature,  $T_{ANN}$ , for Co+FeS milled for 10 h in the weight ratio of 1:1. The as-milled powders were annealed for 0.1 h at  $T_{ANN}$  and subsequently field cooled to room temperature ( $H = 5$  kOe), previously to the magnetic measurements.

## **4.2.- Magnetic properties of $\text{SmCo}_5$ ball milled with NiO and CoO**

### **4.2.1.- Milling time dependence of the coercivity and squareness ratio of as-milled powders**

When  $\text{SmCo}_5 + \text{NiO}$  is subject to heat treatments at temperatures above the  $T_N$  (NiO) to induce FM-AFM coupling, it results in a substantial decrease of  $H_C$ ,  $M_S$  and consequently of  $(BH)_{Max}$ . This effect has a structural origin, rather than a magnetic one. Although the structural changes associated with the heating process have not been examined in detail in the present work, several authors have reported that, when  $\text{SmCo}_5$  is heated to intermediate

temperatures (e.g.  $T \sim 600$  K), there is a progressive loss of its magnetocrystalline anisotropy, mainly due to the segregation of softer phases or even non-magnetic phases, such as  $\text{Sm}_2\text{Co}_{17}$  or  $\text{Sm}_2\text{Co}_7$  [28]. In addition, we have observed that, in annealed  $\text{SmCo}_5 + \text{NiO}$  powders, even when heat treatments are performed under high vacuum conditions ( $10^{-5}$  mbar), Sm is always partially oxidized, probably due to reaction with oxygen from NiO.

Nevertheless, both  $H_C$  and  $M_R/M_S$ , are found to considerably enhance in *as-milled*  $\text{SmCo}_5 + \text{NiO}$  with respect to ball milled  $\text{SmCo}_5$  alone [29-31]. These effects have been attributed to FM-AFM exchange interactions, induced by ball milling, without need of posterior field cooling processes. In this case, the local heating during the milling, due to the impacts between powders and balls, together with the microscopic fields originating from the hard FM  $\text{SmCo}_5$  grains, make it possible to observe some effects of FM:AFM coupling already in the as-milled state, without need of any posterior heat treatment process. Further discussion on this point will be given in annex 5.

However, it is difficult to directly demonstrate the existence of FM-AFM coupling, mainly due to the magnetic and structural character of  $\text{SmCo}_5$  and NiO. Namely, the magnetocrystalline anisotropy of NiO is exceedingly small to allow the existence of significant loop shifts (a clear sign of the existence of FM-AFM coupling) when coupled to  $\text{SmCo}_5$ . Furthermore, the  $\text{SmCo}_5$  structural transitions occurring when heated, even at temperatures much below  $T_N$  (NiO), prevent the analysis of the temperature dependence of the coercivity enhancement (i.e.  $\mathbf{DH}_C$  should disappear at  $T_N$ ). Moreover, the random character of ball-milled powders makes it difficult to search for unidirectional anisotropy using torque magnetometry. Therefore, the existence of FM-AFM has to be proved indirectly. Thus, for comparison, ball milling of  $\text{SmCo}_5 + \text{CoO}$  (CoO with similar initial grain size as NiO) has been also carried out. It is noteworthy that CoO is only AFM at temperatures below room temperature, since  $T_N$  (CoO) = 290 K. Therefore, milling with CoO should not result in  $H_C$  enhancement, since CoO remains paramagnetic during the milling.

The milling time dependence of  $H_C$ , measured at room temperature, for  $\text{SmCo}_5$  milled alone, with NiO and with CoO (in the weight ratio of 1:1) is shown in figure 4.16. The evolution of the magnetic properties of  $\text{SmCo}_5$  when subject to ball milling has been extensively studied by several authors [28,29,32]. As can be seen in the figure, for  $\text{SmCo}_5$  milled alone,  $H_C$  is found to increase with milling time, reaching a maximum value of approximately 11 kOe after 4 h and it decreases afterwards to about 4 kOe after 32 h. The increase of  $H_C$  for short-term milling is attributed to particle size reduction, which converts them from a multidomain to a monodomain state. Nevertheless, when  $\text{SmCo}_5$  is overmilled it tends to become highly disordered, losing part of its high magnetic anisotropy and thus  $H_C$  is reduced.

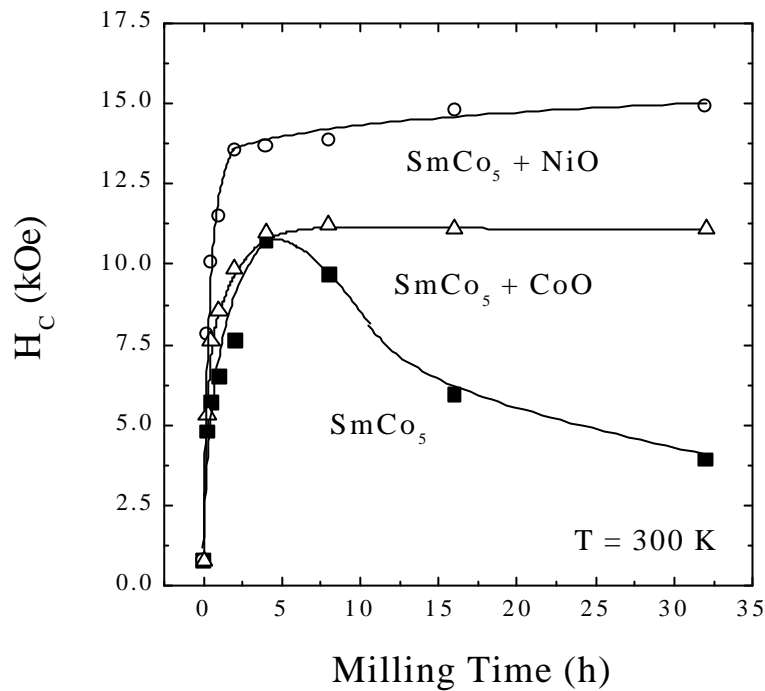


**Figure 4.16:** Milling time dependence of the coercivity,  $H_C$  (measured at room-temperature) for ball-milled  $\text{SmCo}_5$  ( $\blacksquare$ -),  $\text{SmCo}_5 + \text{CoO}$  1:1 ( $\triangle$ -) and  $\text{SmCo}_5 + \text{NiO}$  1:1 ( $\circ$ -) powders. The lines are a guide to the eye.

Although the behavior of the three systems is similar for short milling times, it is clear that already from the early stages of milling an enhancement of  $H_C$  is observed in ball-milled  $\text{SmCo}_5 + \text{NiO}$  in comparison with  $H_C$  values of ball-milled  $\text{SmCo}_5$  and  $\text{SmCo}_5 + \text{CoO}$ . Moreover, in contrast to what is observed for  $\text{SmCo}_5$  alone,  $H_C$  for  $\text{SmCo}_5 + \text{NiO}$  and  $\text{SmCo}_5 + \text{CoO}$  levels off for long milling times. This is because, as has been evidenced by X-ray diffraction results (see section 3.2.4), milling is less aggressive to  $\text{SmCo}_5$  when it is milled together with  $\text{CoO}$  or  $\text{NiO}$ . However, although the microstructure and morphology of  $\text{SmCo}_5 + \text{NiO}$  and  $\text{SmCo}_5 + \text{CoO}$  are rather similar (see section 3.1.2), the former is found to exhibit a much larger  $H_C$ . It is noteworthy that the maximum  $H_C$  in  $\text{SmCo}_5$  milled with  $\text{CoO}$  is approximately the same than in ball milled  $\text{SmCo}_5$  alone.

The fact that  $\text{NiO}$  is antiferromagnetic at room temperature ( $T_N = 590$  K) while  $\text{CoO}$  is paramagnetic ( $T_N = 290$  K), allows the separation of morphological-structural effects from magnetic coupling ones. Since the microstructure in both cases is very similar the enhanced  $H_C$  should be attributed to the existence of a FM-AFM exchange coupling in the  $\text{SmCo}_5 + \text{NiO}$  as-milled powders.

The difference in coercivity can also be observed in figure 4.17, where enlargements of the hysteresis loops for  $\text{SmCo}_5$  milled for 4 h and  $\text{SmCo}_5 + \text{NiO}$  (ratio 1:1) milled for 32 h are shown.

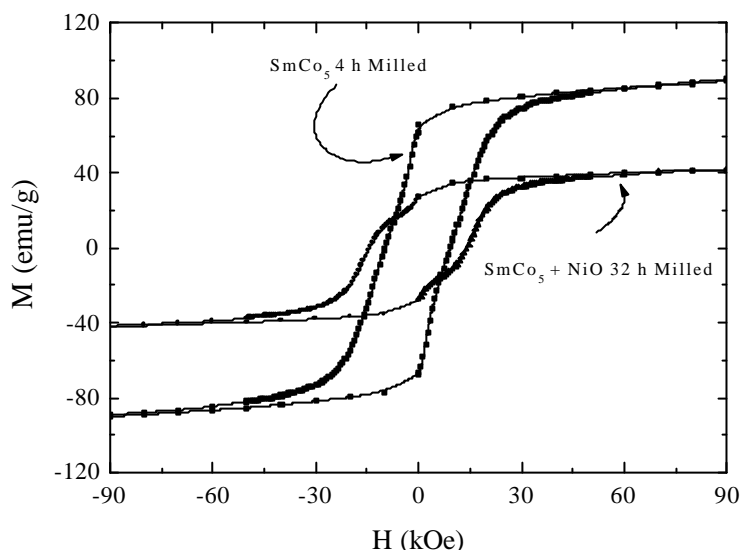


**Figure 4.17:** Enlargements of the hysteresis loops (the maximum field applied was  $H_{Max} = 230$  kOe) of  $\text{SmCo}_5$  and  $\text{SmCo}_5 + \text{NiO}$  ball milled for 4 and 32 h (in the weight ratio of 1:1), respectively.

It can be seen from figure 4.17 that, although the coercivity increases, the saturation magnetization in the case of  $\text{SmCo}_5 + \text{NiO}$  is reduced, due to the zero  $M_S$  of NiO (AFM). Also a shoulder is observed in  $\text{SmCo}_5 + \text{NiO}$  ball milled for 32 h, which is not likely to be due to the presence of two FM phases (XRD patterns show peaks corresponding to only the hard  $\text{SmCo}_5$  phase), but maybe to the existence of different regions with different degrees of coupling between the  $\text{SmCo}_5$  and the NiO particles.

Furthermore, a pronounced enhancement of  $M_R/M_S$  is observed in ball milled  $\text{SmCo}_5$  (either alone or with NiO or CoO), especially after short-term milling. The milling time dependences of  $M_R/M_S$  for the three systems is shown in figure 4.18. Although the Stoner-Wohlfarth model for isotropic, single domain and non-interacting particles predicts a squareness of  $M_R/M_S = 0.5$  [33], values of  $M_R/M_S$  as high as 0.9 are obtained in  $\text{SmCo}_5$  milled for 0.5 h, without aligning the powders previously to magnetic measurements.

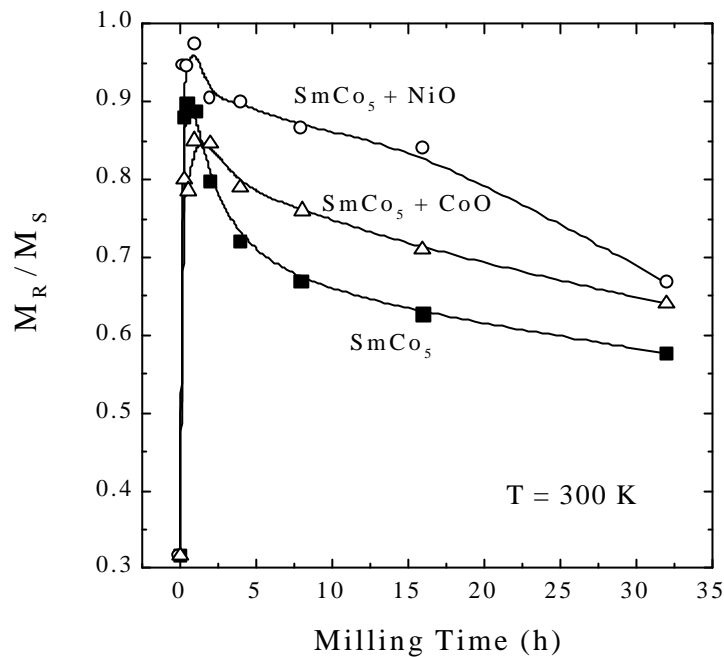


**Figure 4.18:** Milling time dependence of the squareness ratio,  $M_R/M_S$  (measured at room-temperature), for ball-milled  $\text{SmCo}_5$  (-■-),  $\text{SmCo}_5 + \text{CoO}$  1:1 (-△-) and  $\text{SmCo}_5 + \text{NiO}$  1:1 (-○-) powders. The lines are a guide to the eye.

The high values of the squareness ratio are the result of exchange interactions either between the different FM grains [34,35] or between the FM and AFM particles. A study of the evolution and effects of dipolar and exchange interactions on the magnetic properties of as-milled powders, based on the use of the so-called  $\Delta M$  plots, will be presented in section 4.2.3. In addition, an intuitive model about the squareness enhancement due to FM-AFM exchange interactions will be discussed in annex 5. The decrease of  $M_R/M_S$  for long milling times is probably related to some  $\text{SmCo}_5$  structural disorder. The large amounts of dislocations and grain boundaries accumulated after long-term milling probably limit the extent of exchange-coupled regions in the FM and, thus,  $M_R/M_S$  is consequently reduced.

Moreover, as shown in fig. 4.18, short-term milling of  $\text{SmCo}_5 + \text{CoO}$  results in somewhat lower values of  $M_R/M_S$  (compared to  $\text{SmCo}_5$  milled alone or with NiO). Since CoO is paramagnetic at room-temperature, effectively its role is simply to separate the  $\text{SmCo}_5$  particles, thus reducing the exchange interactions between them and thus  $M_R/M_S$ . The crossover at moderate milling times between the  $M_R/M_S$  of  $\text{SmCo}_5 + \text{CoO}$  and  $\text{SmCo}_5$  alone is probably due to the more aggressive effects of the milling on  $\text{SmCo}_5$  alone (see section 3.2).

Contrary to what is observed in ball-milled  $\text{SmCo}_5 + \text{CoO}$ , in  $\text{SmCo}_5 + \text{NiO}$ ,  $M_R/M_S$  values even larger than the ones of  $\text{SmCo}_5$  milled alone are obtained. Hence, the presence of the AFM NiO phase surrounding  $\text{SmCo}_5$  seems to play also some role in further enhancing  $M_R/M_S$ .

#### 4.2.2.- Effect of field cooling to below room temperature on the coercivity of $\text{SmCo}_5$ ball milled with CoO

Further proof that ball milling generates a microstructure favorable for FM-AFM exchange interactions, is obtained from the temperature dependence of  $H_C$  for  $\text{SmCo}_5$  milled alone and together with CoO (during times exhibiting maximum  $H_C$  in each case), after field cooling ( $H_{FC} = 50$  kOe) from room temperature to 30 K (i.e.  $T < T_N(\text{CoO})$ ) (see figure 4.19).

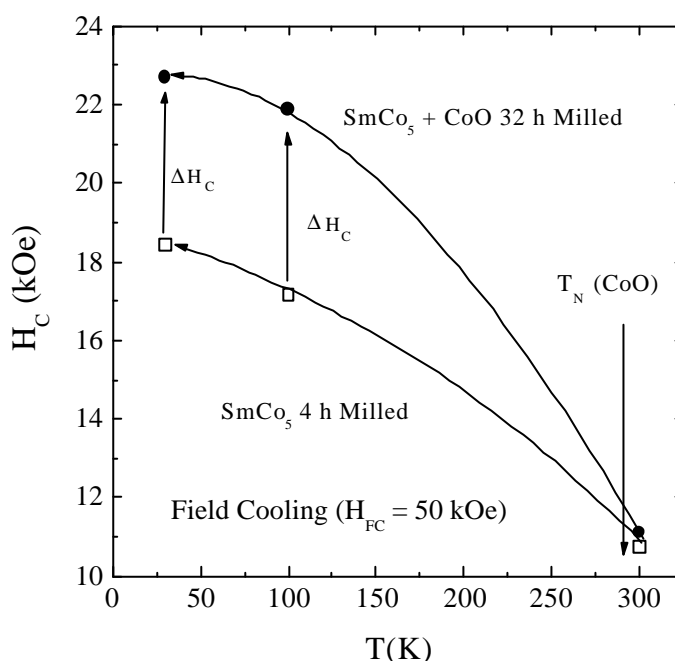


**Figure 4.19:** Temperature dependence of the coercivity,  $H_C$ , for  $\text{SmCo}_5$  ball-milled for 4 h ( $\square$ ) and  $\text{SmCo}_5 + \text{CoO}$  1:1 ball-milled for 32 h ( $\bullet$ ), after field cooling ( $H_{FC} = 50$  kOe) the as-milled powders to 100 K and 30 K. Also indicated is the Néel temperature of CoO ( $T_N = 290$  K). The lines are a guide to the eye.

As can be seen in the figure, when  $\text{SmCo}_5 + \text{CoO}$  (in a weight ratio of 1:1) is field cooled to low temperatures  $H_C$  increases substantially. Part of this increase is due to the changes in magnetocrystalline anisotropy of  $\text{SmCo}_5$ , since a similar increase in  $H_C$  is observed for  $\text{SmCo}_5$  alone. Nevertheless, as expected from the FM-AFM coupling,  $\text{SmCo}_5 + \text{CoO}$

exhibits an extra  $H_C$  enhancement at low temperatures with respect to single  $\text{SmCo}_5$  after the same field cooling procedure (i.e. at  $T = 30$  K, after field cooling from room temperature,  $H_C = 23$  kOe for  $\text{SmCo}_5 + \text{CoO}$ , while  $H_C = 18.5$  kOe for  $\text{SmCo}_5$ ). Moreover, the  $H_C$  enhancement in  $\text{SmCo}_5 + \text{CoO}$  has been found to be less if the cooling is performed in zero field (ZFC). In this case,  $H_C = 20.2$  kOe at  $T = 100$  K, while after field cooling to the same temperature,  $H_C = 22$  kOe. Note that, although the local field of the  $\text{SmCo}_5$  particles can induce FM-AFM coupling to the CoO even after ZFC from a demagnetized state, only those  $\text{SmCo}_5$  particles which are single domain will fully contribute to it. In a field cooling experiment ( $H_{FC} = 50$  kOe) the total magnetic moment of nearly all  $\text{SmCo}_5$  particles spins is aligned parallel to the applied field direction, thus all particles contribute to the coupling.

#### **4.2.3.- Study of the role of FM-FM dipolar and exchange interactions and FM-AFM exchange interactions on $\Delta M$ plots**

Remanence enhancement in isotropic FM particles has also been observed in other ball milled or melt-spun hard magnets, such as NdFeB or SmFeN [36]. This effect is usually related to short-range exchange interactions between ferromagnetic grains [34,35]. These exchange interactions produce a perturbed region, restricted to the grain boundaries, where, once the field is removed, the spins remain oriented in the previous magnetizing field direction, resulting in higher values of  $M_R$ . For  $\text{SmCo}_5$  milled alone,  $M_R/M_S$  reaches its maximum value after 0.5 h of milling and it reduces slowly for longer milling times. This indicates that exchange interactions between FM grains have their maximum effect after short-term milling and tend to decrease afterwards. This reduction is probably due to the introduction of large amounts of defects during the milling, such as dislocations or stacking faults, which limit the extent of exchange-coupled regions within or among the FM particles.

The interactions between the grains in magnetic materials are usually classified as long-range demagnetizing-like magnetostatic (dipolar) interactions and short-range magnetizing-like (exchange) interactions. Both types of interactions are likely to be present in as-milled  $\text{SmCo}_5$ -NiO particles, besides the FM-AFM exchange interactions. To evaluate the strength of the different types of magnetic interactions a procedure known as **DM** plot has been developed [37]. This technique differentiates between two types of remanence curves: the isothermal remanent magnetization curve,  $M_r(H)$ , which is obtained by progressively magnetizing the sample starting from a fully demagnetized state, and the demagnetizing remanent magnetization curve,  $M_d(H)$ , which is obtained by progressively demagnetizing a previously fully saturated sample. In more detail, to measure  $M_r(H)$  one has to apply a small positive magnetic field, remove it and measure the resulting remanent magnetization. This process has to be repeated several times until the magnetic field is large enough to saturate the

sample and the remanence takes the saturation value,  $M_r(\infty)$ . Then, to obtain  $M_d(H)$ , the same procedure has to be carried out starting from the fully saturated state and applying a negative field of increasing strength.  $\mathbf{DM}$  is defined as follows:

$$\Delta M = \frac{M_d(H)}{M_r(\infty)} - \left( 1 - 2 \frac{M_r(H)}{M_r(\infty)} \right) \quad (4.1)$$

Usually, for uniaxial materials, positive  $\mathbf{DM}$  values are interpreted as magnetizing exchange interactions, while negative  $\mathbf{DM}$  correspond to demagnetizing-like magnetostatic interactions [38]. If  $\mathbf{DM}$  is zero, i.e. when  $M_d(H) = M_r(\infty) - 2 M_r(H)$ , the FM particles essentially do not interact with each other [33,39].

The  $\mathbf{DM}$  plots for  $\text{SmCo}_5 + \text{NiO}$  ball-milled for 1, 4 and 32 h are shown in figure 4.20. It can be seen that both types of interactions (magnetostatic and exchange) are present in the material. Positive  $\mathbf{DM}$  values are obtained when the applied field is lower than  $H_C$ , while magnetostatic interactions are predominant for  $H > H_C$ . Similar  $\mathbf{DM}$  plots have also been reported for spring-magnets, where  $M_R/M_S$  is also enhanced when comparing to the hard component [40]. Dipolar interactions tend to decrease with milling time, i.e. the negative peak of the  $\mathbf{DM}$  plots decreases both in width and intensity (and also in area) with milling time. This can be understood in terms of the changes in microstructure of  $\text{SmCo}_5$  particles during the milling process. In fact, dipolar interactions have their main origin in the existence of sharp corners of  $\text{SmCo}_5$  particles, which can create considerable stray field that tend to demagnetize the neighboring particles, thus enhancing dipolar interactions and giving low values of  $M_R/M_S$  on the unmilled  $\text{SmCo}_5$  particles (see figures 3.2 and 4.18). As the milling time increases, the particles tend to become more regular in shape and are also reduced in size. This might explain the reduction of magnetostatic interactions with milling time. However,  $\mathbf{DM}$  plots also indicate that dipolar interactions are still present after even long-term milling.

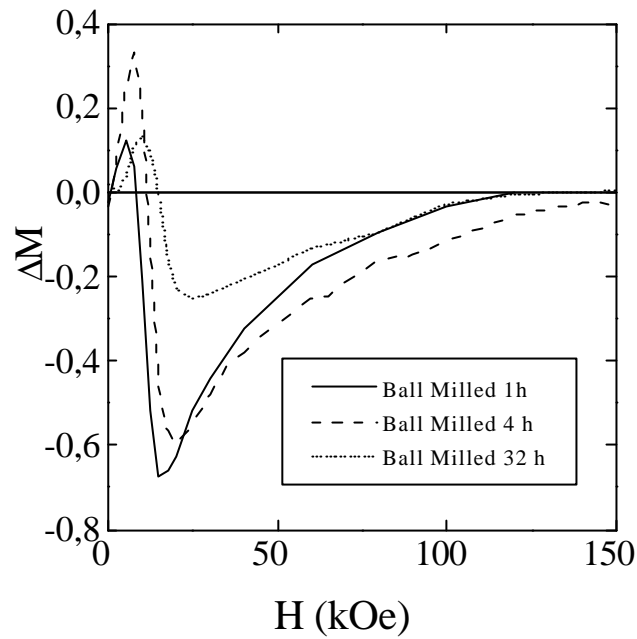


**Figure 4.20:** Milling time dependence of the **DM** curves for SmCo<sub>5</sub> ball milled with NiO for 1 h, 4 h and 32 h.

However, we do not find a direct correlation between the **DM** plots and the milling time dependence of  $M_R/M_S$ , indicating that exchange interactions develop during the milling in a complex way. For example, although the field range in which exchange interactions predominate increases with the milling time, i.e. the width of the positive peak in the **DM** plots increases monotonously with milling time, the area of the positive peak becomes maximum after intermediate milling times (e.g. 4 h). On the contrary, maximum  $M_R/M_S$  values correspond to short milling times (e.g. 0.5 h). Although we do not have yet a full understanding of this apparent contradiction, it is likely to be due to the interplay between effects of FM-FM exchange and FM-AFM exchange interactions which simultaneously affect the shape of the **DM** curves.

A simpler way to quantify the strength of the interactions using a single parameter is by the so-called interaction field factor (*IFF*), which is defined from  $H_C$  and the remanence coercivities,  $H_r$  and  $H_r'$  (where:  $M_d(H_r) = 0$  and  $M_r(H_r') / M_r(\infty) = 1/2$ ), as follows [41]:

$$IFF = \left[ \frac{(H_r' - H_r)}{H_c} \right] \times 100 \quad (4.2)$$

The *IFF* would be expected to be zero for non-interacting single domain particles and to increase as the interactions become more important. Shown in table 4.2 are the milling time dependences of *IFF*, together with those of the  $\text{SmCo}_5$  crystallite size ( $\langle D \rangle_{\text{SmCo}_5}$ ), NiO crystallite size ( $\langle D \rangle_{\text{NiO}}$ ),  $\text{SmCo}_5$  microstrain ( $\langle \epsilon^2 \rangle_{\text{SmCo}_5}^{1/2}$ ) and also, for easier comparison,  $H_c$  and  $M_R/M_S$ , for ball-milled  $\text{SmCo}_5 + \text{NiO}$ .

Milling Times	$\langle D \rangle_{\text{SmCo}_5}$ (nm)	$\langle D \rangle_{\text{NiO}}$ (nm)	$\langle \epsilon^2 \rangle^{1/2}$	$H_c$ (kOe)	$M_R/M_S$	<i>IFF</i> (%)
1 h	20	27	0.004	11.3	0.98	38.3
4 h	18	22	0.007	13.3	0.90	16.1
32 h	9	11	0.010	15	0.67	10.8

**Table 4.2:** Summary of the structural and magnetic properties for  $\text{SmCo}_5 + \text{NiO}$  ball-milled for 1 h, 4h and 32 h.

It is remarkable that, as mentioned,  $M_R/M_S$  reaches its maximum value after 1 h of milling and it reduces slowly for longer milling times. This indicates that exchange interactions between FM grains have their maximum effect after 1 h of milling and tend to decrease afterwards, probably due to the introduction of large amounts of defects, such as dislocations or stacking faults, during the milling (see high microstrain values in table 4.2), which reduce the extent of the exchange coupled regions in the FM. This correlates well with the milling time dependence of *IFF*. However, exchange interactions between the FM and the AFM particles are expected to increase with the milling time, since prolonged milling favors a larger amount of interfaces to be formed between  $\text{SmCo}_5$  and NiO. Thus, the competition between the FM-FM and the FM-AFM exchange interactions, which have opposite tendencies during the milling, could explain the non-monotonic behavior of the positive peak in the **DM** plots. However, due to the interplay among FM-FM exchange and dipolar interactions and the AFM-FM exchange interactions, the correlation between  $M_R/M_S$  enhancement and the **DM** plots is not found straightforward.

#### 4.2.4.- Effect of FM-AFM percentages on the coercivity and energy product enhancements

In order to elucidate the role of NiO in the energy product enhancement, ball milling of  $\text{SmCo}_5$  with NiO has been carried out varying the proportions of FM and AFM [30]. The milling time dependence of  $H_C$  for  $\text{SmCo}_5$  milled with NiO in the weight ratios of  $\text{SmCo}_5$  (1):(0) NiO,  $\text{SmCo}_5$  (3):(1) NiO,  $\text{SmCo}_5$  (3):(2) NiO and  $\text{SmCo}_5$  (1):(1) NiO is shown in fig. 4.21.

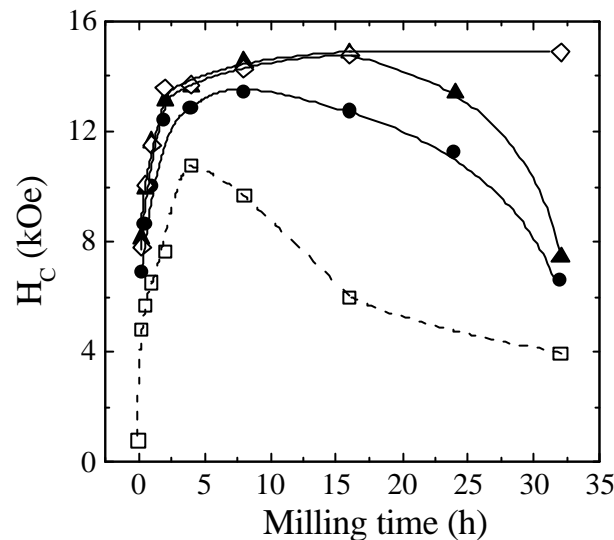


**Figure 4.21:** Milling time dependence of the coercivity,  $H_C$ , for  $\text{SmCo}_5$  milled with NiO in the weight ratios  $\text{SmCo}_5$  (1):(0) NiO ( $\text{---} \square \text{---}$ ),  $\text{SmCo}_5$  (3):(1) NiO ( $\text{---} \bullet \text{---}$ ),  $\text{SmCo}_5$  (3):(2) NiO ( $\text{---} \blacktriangle \text{---}$ ) and  $\text{SmCo}_5$  (1):(1) NiO ( $\text{---} \diamond \text{---}$ ). Note that the error bars are smaller than the symbols. The lines are a guide to the eye.

It can be seen that the maximum  $H_C$  is found to increase with the NiO content. This can be explained in terms of the microstructure developed in the composites. It has been observed that the  $\text{SmCo}_5 + \text{NiO}$  agglomerates, where FM-AFM exchange interactions are more likely to take place, form more easily for higher AFM contents. Besides, the milling time at which  $H_C$  exhibits its maximum value shifts towards higher values as the NiO content is increased. This is due to the role of NiO in slowing down  $\text{SmCo}_5$  structural changes, thus delaying the decrease of  $H_C$  (see section 3.2).

The milling time dependence of the squareness ratio,  $M_R/M_S$ , for  $\text{SmCo}_5$  milled alone and with NiO, in several weight ratios, is shown in figure 4.22.

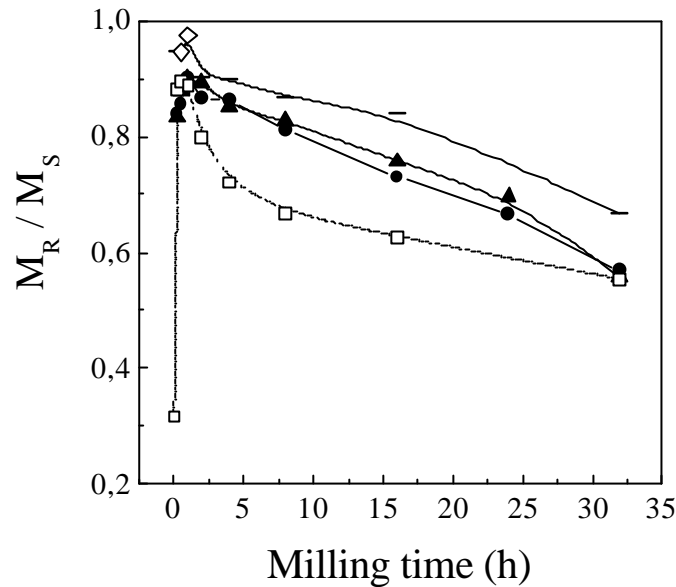


**Figure 4.22:** Milling time dependence of the squareness ratio,  $M_R/M_S$ , for  $\text{SmCo}_5$  milled with NiO in the weight ratios  $\text{SmCo}_5$  (1):(0) NiO (—□—),  $\text{SmCo}_5$  (3):(1) NiO (—●—),  $\text{SmCo}_5$  (3):(2) NiO (—▲—) and  $\text{SmCo}_5$  (1):(1) NiO (—◇—). Note that the error bars are smaller than the symbols. The lines are a guide to the eye.

For all compositions, the maximum values of  $M_R/M_S$  are obtained after short-term milling, i.e. between 0.5 and 1 h, and a progressive decrease of  $M_R/M_S$  is observed for longer milling times. However, mainly for all milling times, higher values of  $M_R/M_S$  are observed for larger NiO contents. This is due to FM-AFM exchange interactions but, also, to the role of NiO in slowing down  $\text{SmCo}_5$  structural changes occurring during the milling. Since the deterioration of  $\text{SmCo}_5$  microstructure is slower as the NiO content increases, the decrease of  $M_R/M_S$  is also slowed down. However, note that, even after long-term milling, the values of  $M_R/M_S$  remain higher than 0.5 (which is the Stoner-Wolfarth theoretical value for non-oriented, single-domain, non-interacting particles [33]). This indicates that, in spite of large amounts of structural defects, many FM grains still remain exchange coupled after long milling times [34,35].

The milling time dependence of  $(BH)_{Max}$  is shown in fig. 4.23 for the different FM:AFM ratios. It can be observed that the dependence of  $(BH)_{Max}$  on the AFM content is rather complex. This is because of the opposing effects of the AFM in the enhancement of  $(BH)_{Max}$ .

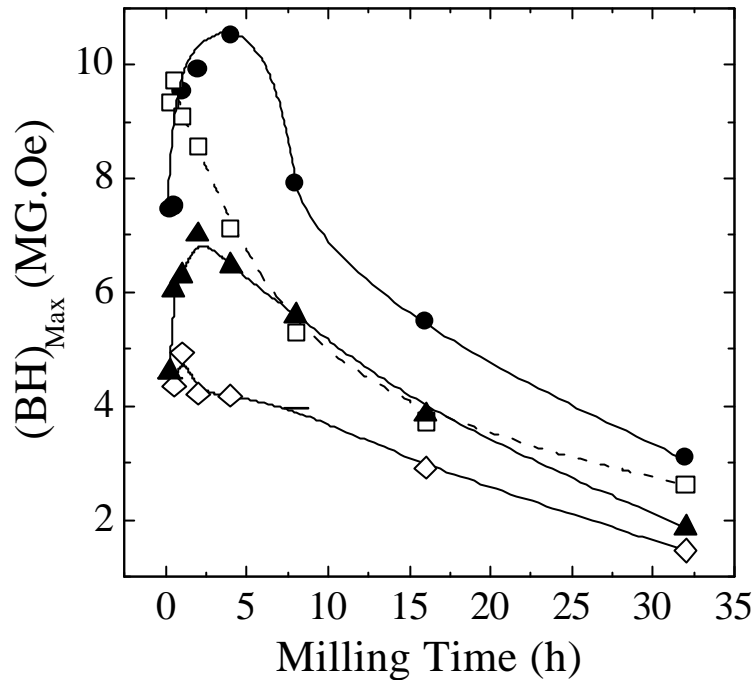


**Figure 4.23:** Milling time dependence of the energy product,  $(BH)_{Max}$ , for  $\text{SmCo}_5$  milled with NiO in the weight ratios  $\text{SmCo}_5$  (1):(0) NiO (—□—),  $\text{SmCo}_5$  (3):(1) NiO (—●—),  $\text{SmCo}_5$  (3):(2) NiO (—▲—) and  $\text{SmCo}_5$  (1):(1) NiO (—◇—). Note that the error bars are smaller than the symbols. The lines are a guide to the eye.

On the one hand, both  $H_C$  and  $M_R/M_S$  increase due to the FM-AFM and FM-FM exchange interactions respectively (as for ball milled Co + NiO). On the other hand, the presence of NiO results in a reduction of the saturation magnetization of the composite, proportional to the NiO content. This stems from the zero net magnetization of the AFM ( $M_{AFM} = 0$ ), which does not contribute to the overall saturation magnetization. Consequently, as seen in fig. 4.23,  $(BH)_{Max}$  is reduced for all milling times when the NiO content is increasingly high, as for example in the case of the 1:1 ratio. Nevertheless,  $(BH)_{Max}$  for the  $\text{SmCo}_5$  (3):(1) NiO milled for 4 h exhibits an enhancement with respect to the maximum of pure  $\text{SmCo}_5$ . However, due to the interplay of all the different effects, an enhancement of  $(BH)_{Max}$  can only be achieved through the optimization of milling time and the FM:AFM weight ratio.

## References

- [1] J. Sort, J. Nogués, X. Amils, S. Suriñach, J.S. Muñoz, M.D. Baró, Appl. Phys. Lett. **75** (1999) 3177.
- [2] J. Sort, J. Nogués, X. Amils, S. Suriñach, J.S. Muñoz, M.D. Baró, J. Magn. Magn. Mater. **219** (2000) 53.
- [3] J. Sort, J. Nogués, X. Amils, S. Suriñach, J.S. Muñoz, M.D. Baró, Mat. Sci. Forum **343-346** (2000) 812.
- [4] J. Sort, J. Nogués, X. Amils, S. Suriñach, J.S. Muñoz, M.D. Baró, Mat. Res. Soc. Symp. Proc. **581** (2000) 641.
- [5] D. Weller, G. R. Harp, R.F.C. Farrow, A. Cebollada, J. Sticht, Phys. Rev. Lett. **72** (1994) 2097.
- [6] J. Nogués, I.K. Schuller, J. Magn. Magn. Mater. **192** (1999) 203
- [7] D. A. Young, *Phase diagrams of the Elements* (University of California Press, Berkeley, 1991).
- [8] O. Kitakami, H. Sato, Y. Shimada, F. Sato, M. Tanaka, Phys. Rev. B **56** (1997) 13849.
- [9] T. Ambrose, C.L. Chien, J. Appl. Phys. **83** (1998) 6822; T. Ambrose, C.L. Chien, J. Appl. Phys. **83** (1998) 7222.
- [10] S. Soeya, T. Imagawa, K. Mitsuoka, S. Narishige, J. Appl. Phys. **76** (1994) 5356.
- [11] P.J. van der Zaag, A.R. Ball, L.F. Feiner, R.M. Wolf, P.A.A. van der Heijden, J. Appl. Phys. **79** (1996) 5103.
- [12] K. Hoshino, S. Noghehi, R. Nakatani, H. Hoshiya, Y. Sugita, Jpn. J. App. Phys. **33** Part 1 (1994) 1327.
- [13] J. Löffler, W. Wagner, H. Van Swygenhoven, J. Meier, B. Doudin, J. P. Ansermet, Mater. Sci. Forum **235-238** (1997) 699; Y. D. Yao, Y. Y. Chen, M.F. Tai, D. H. Wang, H. M. Lin, Mater. Sci. Eng. A **217/218** (1996) 281.
- [14] H. S. Cho, F. Ueda, C. Huo and H. Fujiwara, IEEE Trans. Magn. **34** (1998) 1414; S. F. Cheng, J. P. Teter, P. Lubitz, M. M. Miller, L. Hoines, J. J. Krebs, D. M. Schaefer and G. A. Prinz, J. Appl. Phys. **79** (1996) 6234.
- [15] B. Gustard, W. J. Schuele, J. Appl. Phys. **37**, 1168 (1966).

- [16] I.S. Jacobs, *J. Appl. Phys.* **32** (1961) 61S.
- [17] K.W. Blazey, H. Rohrer, R. Webster, *Phys. Rev. B* **4** (1971) 2287.
- [18] K. Kurosawa, M. Miura, S. Saito, *J. Phys. C: Solid St. Phys.* **13** (1980) 1521.
- [19] J. Nogués, L. Morellon, C. Leighton, M.R. Ibarra, I.K. Schuller, *Phys. Rev. B* **61** (2000) R6455.
- [20] G.C. Hadjipanayis, *J. Magn. Magn. Mater.* **200** (1999) 373.
- [21] S. Soeya, S. Nakamura, T. Iamgawa, S. Narishige, *J. Appl. Phys.* **77** (1995) 5838.
- [22] W.H. Meiklejohn, C.P. Bean, *Phys. Rev.* **102** (1956) 1413; W.H. Meiklejohn, C.P. Bean, *Phys. Rev.* **105** (1957) 904; W.H. Meiklejohn, *J. Appl. Phys.* **29** (1958) 454.
- [23] S.H. Charap, E. Fulcomer, *J. Appl. Phys.* **42** (1971) 1426; E. Fulcomer, S.H. Charap, *J. Appl. Phys.* **43** (1972) 4190.
- [24] F.B. Hagedorn, *J. Appl. Phys.* **38** (1967) 3641.
- [25] M. Tsunoda, Y. Tsuchiya, M. Konoto, M. Takahashi, *J. Magn. Magn. Mater.* **171** (1997) 29.
- [26] C. Tsang, K. Lee, *J. Appl. Phys.* **53** (1982) 2605.
- [27] J. Fujikata, K. Hayashi, H. Yamamoto, M. Nakada, *J. Appl. Phys.* **83** (1998) 7210.
- [28] K. J. Strnat and R. M. W. Strnat, *J. Magn. Magn. Mater.* **100** (1991) 38.
- [29] J. Sort, J. Nogués, S. Suriñach, J.S. Muñoz, M.D. Baró, E. Chappel, F. Dupont, G. Chouteau, *Appl. Phys. Lett.* **79** (2001) 1142.
- [30] J. Sort, S. Suriñach, J.S. Muñoz, M.D. Baró, J. Nogués, G. Chouteau, V. Skumryev, G.C. Hadjipanayis, *Phys. Rev. B* **65** (2002) 174420.
- [31] J. Sort, J. Nogués, S. Suriñach, J.S. Muñoz, E. Chappel, F. Dupont, G. Chouteau, M.D. Baró, *Mat. Sci. Forum* **386-388** (2002) 465.
- [32] D. L. Leslie-Pelecky, E. M. Kirkpatrick, and R. L. Schalek, *Nanostruct. Mater.* **12** (1999) 887; D. L. Leslie-Pelecky and R. L. Schalek, *Phys. Rev. B* **59** (1999) 457.
- [33] E. C. Stoner, E. P. Wohlfarth, *Philos. Trans. R. Soc. A* **240** (1948) 599.
- [34] A. Hernando, I. Nabarro, J.M. González, *Europhys. Lett.* **20** (1992) 175.

- [35] T. Schrefl, J. Fidler, H. Kronmüller, *Phys. Rev. B* **49** (1994) 6100.
- [36] R. Coehoorn, D.B. de Mooij, C. de Waard, *J. Magn. Magn. Mater.* **80** (1989) 101; P.J. McGuinness, S. Kobe, *J. Alloys Comp.* **281** (1998) 23; J. Wecker, M. Katter, L. Schultz, *J. Appl. Phys.* **69** (1991) 6058.
- [37] P. E. Kelly, K. O'Grady, P. I. Mayo, R. W. Chantrell, *IEEE Trans. Magn.* **25** (1989) 392.
- [38] R. W. Gao, D. H. Zhang, W. Li, X. M. Li, J. C. Zhang, *J. Magn. Magn. Mater.* **208** (2000) 239; M. P. Morales, K. O'Grady, B. Zhang, Wayne R. Bennett, G. C. Rauch, *IEEE Trans. Magn.* **32** (1996) 3593.
- [39] J. García-Otero, M. Porto, J. Rivas, *J. Appl. Phys.* **87** (2000) 7376.
- [40] I. Panagiotopoulos, L. Withanawasam, G. C. Hadjipanayis, *J. Magn. Magn. Mater.* **152** (1996) 353; Z. Chen, H. Okumura, G. C. Hadjipanayis, Q. Chen, *J. Appl. Phys.* **89** (2001) 2299.
- [41] A. R. Corradi, E. P. Wohlfarth, *IEEE Trans. Magn.* **14** (1978) 861.